

University of Alberta

Tailoring sorption properties of nano-sized multilayer structured magnesium for
hydrogen storage

by

Ramin Zahiri Sabzevar

A thesis submitted to the Faculty of Graduate Studies and Research
in partial fulfillment of the requirements for the degree of

Master of Science

in Materials Engineering

Department of Chemical and Materials Engineering

© Ramin Zahiri Sabzevar

Fall 2012

Edmonton, Alberta

Permission is hereby granted to the University of Alberta Libraries to reproduce single copies of this thesis and to lend or sell such copies for private, scholarly or scientific research purposes only. Where the thesis is converted to, or otherwise made available in digital form, the University of Alberta will advise potential users of the thesis of these terms.

The author reserves all other publication and other rights in association with the copyright in the thesis and, except as herein before provided, neither the thesis nor any substantial portion thereof may be printed or otherwise reproduced in any material form whatsoever without the author's prior written permission

Dedication

This work is dedicated to my Mom, Dad, Maryam and Ben. Thank you.

Abstract

To tailor the hydrogen sorption properties of magnesium, improve its poor kinetics and alter its thermodynamics properties, sputtered multilayer Mg-based thin films were prepared in which Mg layers were confined by AlTi layers. Multilayer samples of different Mg thickness showed relatively long activation periods compared to the conventional co-sputtered alloys thin films. This activation period is attributed to the formation of voids and new surfaces which facilitate hydrogen transportation and its interaction with base metal. It has been found that the cyclability performance of materials is strictly connected to the stability of microstructure and resistance of multilayer structure to grain growth. At a certain Mg:AlTi thickness ratio (10:2), sintering of Mg layer could be prevented and long cyclability over 250 cycles has been achieved. Multilayers of few nm Mg thicknesses possess equilibrium pressures higher than pure Mg and the plateau pressure is a function of Mg thickness.

Acknowledgments

First and foremost, I would like to thank Dr. David Mitlin, my academic supervisor, who fully supported me to accomplish this research. He helped me develop my skills during course of research and hurdle obstacles in the completion of this project. I greatly appreciate his attitude and unconditional support.

I am also grateful to my friends in Dr. Mitlin's group who never deprived me of their insightful opinions and help. Many thanks to Dr. Babak Shalchi, Beniamin Zahiri, Brian Olsen, Chris Holt, Dr. Peter Kalisvaart, XueHai Tan and Dr. Mohsen Danie.

Finally, I appreciate NINT staff who extended their valuable assistance in operation of tools. Great thanks to Steve Launspach and Martin Kupsta.

Contents

1 INTRODUCTION	1
1.1 HYDROGEN ENERGY	1
1.2 HYDROGEN STORAGE	2
1.3 METAL HYDRIDES	4
1.3.1 INTERACTION OF HYDROGEN WITH SURFACE	5
1.3.2 PENETRATION AND DIFFUSION OF HYDROGEN INSIDE METALLIC MATRIX	8
1.3.3 THERMODYNAMICS OF METAL HYDRIDES FORMATION	10
1.4 MAGNESIUM HYDRIDE	16
1.5 SCOPE OF THIS PROJECT	19
1.6 REFERENCES	20
2 MICROSTRUCTURAL EVOLUTION DURING LOW TEMPERATURE SORPTION CYCLING OF MG-ALTI MULTILAYER NANOCOMPOSITES	26
2.1 INTRODUCTION	26
2.2 EXPERIMENTAL TECHNIQUES	29
2.3 RESULTS	31
2.3.1 KINETICS	31
2.3.2 THERMODYNAMICS	35
2.3.3 MICROSTRUCTURAL ANALYSIS	37
2.4 DISCUSSION	43
2.5 SUMMARY	50
2.6 REFERENCES	51
3 THERMODYNAMICS DESTABILIZATION OF MG-BASED MULTILAYERS FOR HYDROGEN STORAGE	57
3.1 INTRODUCTION	57
3.2 EXPERIMENTAL	61
3.3 RESULTS AND DISCUSSION	63
3.4 SUMMARY	70
3.5 REFERENCES	71
4 CONCLUSIONS	75

List of figures

Figure 1-1 An ideal closed energy cycle starting with hydrogen production using solar energy, moving through storage and finishing with delivery for consumption [3]. 2

Figure 1-2 The potential energy curve demonstrates corresponding energy barriers for interaction of hydrogen with two different metals, one with positive (Endothermic) and the other with negative (exothermic) heat of solution ΔH_{sol} [adopted from [21]]. 6

Figure 1-3 Plot of logarithmic rate constant vs reciprocal temperature. 10

Figure 1-4 Pressure-composition isotherms diagram for a typical Metal-Hydride transformation (a) and corresponding van't Hoff plot (b). 10

Figure 1-5 Energy diagram for (de)hydrogenation of metal (metal hydride). When catalyzed, the energy barrier decreases for both absorption and desorption. When destabilized, the temperature can be reduced for desorption due to less stable bonding between metal and hydrogen [adapted from [20]]. 16

Figure 2-1 Absorption and desorption behavior of 10/2 (A,C), co-sputtered 20/2 (B,D) multilayer samples. 32

Figure 2-2 Absorption and desorption behavior of 20/2 (A,C) and 34/2 (B,D) multilayer samples. 33

Figure 2-3 The time to reach 90% of average maximum capacity as a function of cycle number for (A) absorption and (B) desorption. 34

Figure 2-4 Pressure-composition isotherms of (A) cosputtered 20/2 and (B) 10/2 multilayers. 36

Figure 2-5 (A) Bright field and (B) dark field images and (C) corresponding SAD of 10/2 multilayer after 10 cycles. The SAD shows a [121] zone axis of Mg and the bright field is taken using (010) reflection. (D) HRTEM image shows intimate contact between Mg atomic planes and AlTi amorphous/nanocrystalline layers. (E) Cross section image of as-prepared 10/2 multilayer. 38

Figure 2-6 (A) X-ray diffraction patterns of the studied multilayer composites after cycling; (B) a comparison between as deposited samples 20/2 and co-sputtered 20/2 showing the shift in Mg(002) crystalline peak from 34.3 to 35 due to formation of metastable solid solution between Mg, Al and Ti through sputtering; (C) XRD pattern of a multilayer sample with extra thick (50 nm) Al-Ti layer after 121 sorption cycles before and after cycling to highlight the AlTi intermetallic nanocrystalline/amorphous hump. The inset in (C) shows XRD scan of a 50 nm co-sputtered Al-Ti film treated at same condition as the multilayers in absorbed state. 39

Figure 2-7 Variation of MgH₂ grain size as a function of cycle number. 41

Figure 2-8 SEM images of cycled composites: (A) macroscopic view of 10/2 showing multilayer films preserving their original shapes, (B) FIB image of the cross section showing expansion and void formation between the AlTi layers and a few particles diffused through the AlTi layers and coalesced; (C) macroscopic view of co-sputtered 20/2 showing multilayer films preserving their original shapes, (D) FIB image of the cross sectional view of co-sputtered 20/2 showing void formation between the AlTi layers. 44

Figure 2-9 (A) macroscopic view of 20/2 multilayer showing some disintegration in original films shapes, (B) FIB image of the cross section view of 20/2 showing severe expansion and void formation between the AlTi layers and deformation and rupture of AlTi layers while new large interlayer particles formed; (C) macroscopic view of 34/2 showing original films disintegrated into small flakes, (D) microscopic top view of the 34/2 flakes showing spongy structure after cycling. 46

Figure 2-10 (A,C) Bright-field and (B,D)high angle annular dark field images of co-sputtered 20/2 sample after 60 cycles along with the elemental mapping of Mg, Ti and Al (E,F,G). 47

Figure 2-11 (A) STEM Bright-field and (B) high angle annular dark field images of a Mg particle of co-sputtered 20/2 sample after 260 cycles along with the elemental mapping of Mg, Ti and Al. 49

Figure 3-1 XRD patterns of as deposited Mg/AlTi samples of different configurations. At very thin thicknesses the preferred orientation for Mg changes from $\langle 0\ 2\ 2 \rangle$ to $\langle 0\ 1\ 1 \rangle$ (a) XRD patterns of as deposited 2/2 and 5/2 nm Mg/Ti samples (b) XRD patterns of Mg/AlTi samples after first absorption (c) and XRD patterns of 5/2 Mg/Ti after first absorption and first desorption (d). 64

Figure 3-2 Absorption pressure – temperature isotherms of Mg-AlTi samples of three different Mg thicknesses (d) with constant AlTi thickness of 2 nm at 473 K (A) and the corresponding $\ln(P)$ as a function of $1/d$ (B). 65

Figure 3-3 Absorption PCT of three multilayers with the Mg layers thickness constant at 5 nm and AlTi layers of 0.5, 2, and 8 nm measured at 473 K. 67

Figure 3-4 Absorption pressure – temperature isotherms of Mg-Ti samples of three different Mg thicknesses (d) with constant Ti thickness of 2 nm at 473 K (A) and the corresponding $\ln(p)$ as a function of $1/d$ (B). 68

Figure 3-5 Desorption PCT of Mg/AlTi (2/2) and Mg/Ti (2/2) at 473 K (A). A SEM image of 2/2 Mg/AlTi after first absorption (B). 69

Figure 3-6 Absorption PCT of 0.5/0.5 Mg/AlTi measured at 293 K corresponding with enthalpy of 48 kJ/mole H₂ (A). Absorption (B) and desorption (C) curve at 293 K and 423 K respectively. 70

List of Symbols

μ	Chemical potential
P	Pressure
T	Temperature
θ	Coverage ratio
c	Concentration
H	Enthalpy
S	Entropy
R	Universal gas constant
f	Fraction reacted
t	Time
f	Degree of freedom
b	Number of interstitial sites
D	Grain size (Average diameter)
e	Microstrain
k_B	Boltzman constant
K(P)	Rate constant (pressure dependant)
K(T)	Rate constant (temperature dependant)
k	Rate constant
K	Equilibrium constant
γ	Interface energy
λ	Wavelength
V	Molar volume
r	Diameter
M	Mass
h	Plank constant
A	Area
α	Alpha phase
ϵ	Binding energy
E	Activation energy

1 Introduction

1.1 Hydrogen Energy

The global concerns regarding the use of fossil fuels include their scarcity and environmental impact. This has led to a search for a cleaner and more abundant source of energy to eliminate or reduce greenhouse gas emissions. Hydrogen and fuel cell technologies are considered by many as promising energy system solutions to provide sustainable energy. The by-product of hydrogen combustion, whether it is used in combustion engines or in fuel cells, is water, which is not harmful to environment [1, 2].

The closed energy chain for hydrogen system starts from its production, passes through storage and ends up with its utilization (figure 1-1) [3]. Hydrogen is mainly produced from natural gases and coal through steam reforming. The main problem of this method is CO₂ emission. Other techniques are electrolysis of water and photolytic splitting using electricity produced from renewable resources such as wind and solar energy, or from high-temperature thermochemical cycles of biomass [4]. In the second step, hydrogen needs to be stored, a key challenge for most of on-board applications. Basically, hydrogen storage requires reduction in volume of hydrogen gas, since a small amount of hydrogen occupies considerable volume. In order to increase hydrogen density in a storage system, hydrogen storage technologies have been developed. Compressing hydrogen to high pressures or decreasing the temperature below critical gas temperature can be applied for storage. Another way

to store hydrogen is to reduce repulsion between hydrogen molecules by reaction with other materials. In this case, hydrogen can be stored in a relatively low volume. Irrespective of the method used to store hydrogen, an ideal hydrogen storage medium should be able to be reversibly charged and discharged over 1000 cycles without considerable cost or material degradation [5].

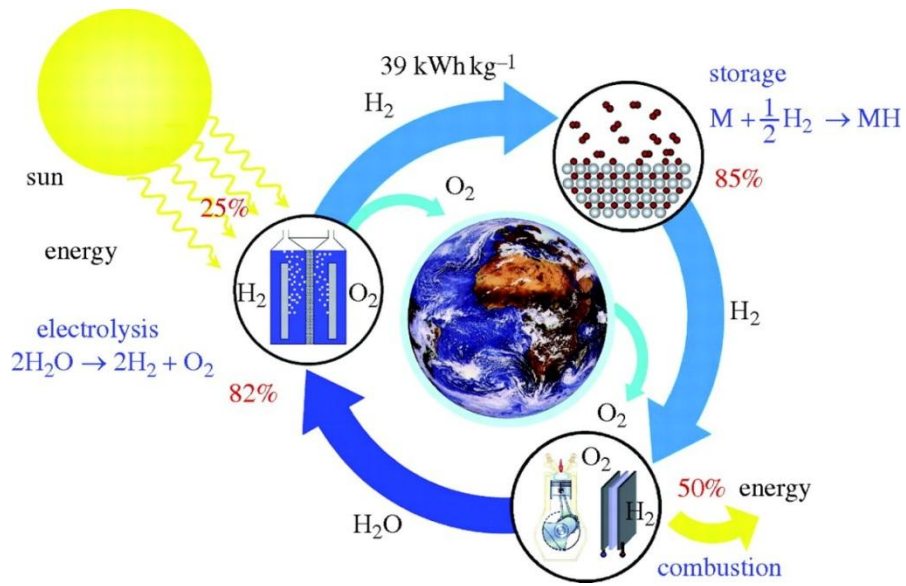


Figure 1-1 An ideal closed energy cycle starting with hydrogen production using solar energy, moving through storage and finishing with delivery for consumption [3].

1.2 Hydrogen storage

Hydrogen has the highest energy per mass of material, a value three times higher than gasoline. However, its low volumetric density, low temperature of liquefaction and its destructive influence on the properties of most design material leads to demand for development of safe and efficient storage systems. Most particularly for

on-board applications such automobile, it is very demanding to store sufficient amount of hydrogen to fuel the automobile [6]. Traditionally, hydrogen is physically stored in gaseous form in steel cylinders, or as a liquid in cryogenic tanks. Both methods have their own drawbacks. In the case of hydrogen gas compression, energy required for reaching high operating pressures and cost of lightweight high strength materials are still high. Additionally, safety issue is still a concern. Boil-off is the major problem in liquid hydrogen tanks which leads to hydrogen loss [5, 6]. Alternatively, in chemical methods for hydrogen storage, hydrogen is adsorbed or absorbed into the structure of suitable materials. In this case, hydrogen is released under certain conditions, depending on the materials' sorption properties. Metal hydrides, chemical hydrides and carbon-based materials are mostly used media in chemical storage methods. The high surface area of some forms of carbon materials allow to hydrogen molecules to adsorb on the surfaces. Usually, low temperatures and high pressure are required for making such a weak bonding. As a result of reaction of chemical hydrides with water or alcohol, hydrogen can be released. However, in most cases the reaction is not reversible. This is while the reaction is reversible for most metal hydrides.

While physical methods of hydrogen storage have been well developed and utilized for practical applications, they do not still meet all requirements of DOE (Department of Energy) 2015 targets which is 6 wt. hydrogen capacity [7]. Hydrogen even in high pressure gas cylinders (e.g. 70 MPa tanks) still has a much lower energy density than that of gasoline. One liter gasoline has six times higher energy compared

to one liter hydrogen compressed to 700 bar. Furthermore, increasing the hydrogen pressure in cylinders to increase the volumetric capacity is sacrificed with reduction in gravimetric capacity (the amount of hydrogen stored per mass of material) as thicker walls are required [8]. Although currently high pressure cylinders can be made of lightweight carbon fibers which provide sufficient gravimetric capacity, the material itself is costly [9]. Metal hydrides are very interesting for hydrogen storage because of number of hydrogen atoms per metal atom, i.e., having high volumetric capacity. They can reversibly store hydrogen, and if chosen from lightweight metals, they can provide high amount of hydrogen per mass (> 7 wt%).

1.3 Metal Hydrides

Hydrogen storage in metal hydrides is a high volume and safe storage method. As a result of chemical reaction of hydrogen with metal, hydrides are formed. The heat released or absorbed during reaction is a characteristic of metal hydride and indicates how weak or strong the bonding between the metal and the hydrogen is. An ideal storage material needs to have: high gravimetric and volumetric capacity, good cyclability and reversibility, low dissociation temperature and pressure, good thermal conductivity for heat transfer and fast kinetics. Currently, no candidate has been found to meet all above requirements; however research studies are being focused on the improvement of properties of known candidates or on developing new materials.

Group I and II elements of periodic table form hydrides with covalent or ionic bonding characteristics. These types of metal form stable hydrides, and dehydrating

only takes place at high temperatures. Among all, lithium and magnesium-based hydrides have been the focus of most studies. In contrast to group I and II, the transition metals forms metallic bonds with hydrogen at high hydrogen pressures. Transition metals are known for their intrinsic property in dissociation of hydrogen and forming unstable hydride. Because of this property, studies have been conducted on the addition of TMs to light weight metal hydride such as MgH_2 . In this regard, many researchers have proven the ability of TMs to tailor the kinetics and thermodynamics of light weight hydrides [10, 11, 12, 13]. Mg_2Cu is an example of a destabilized hydride in which the addition of Cu to Mg results in formation of a less stable hydride. The plateau pressure of 1 bar occurs at 240 °C for Mg_2Cu , however the isotherm is around 280 °C at the same pressure for pure MgH_2 [14].

Hydrogen storage in metals is a complex process and several steps are involved in this process. Each step may govern the overall kinetics of reaction. In this case, surface and bulk characteristics of solid materials play an important role in dictating the sorption properties, in terms of both kinetics and thermodynamics. Understanding the fundamental of metal-hydrogen reaction and also the thermodynamics of metal to hydride transformation help us select appropriate approach toward tailoring sorption properties of hydrogen storage materials.

1.3.1 Interaction of hydrogen with surface

The hydrogen interaction with a metal consists of several steps each of which has its own characteristics energy barrier. Applying the Lennard-Jones potential [15], one

can describe these steps in a single one-dimensional potential energy curve as seen in figure 1-2. Depending on the condition, i.e. temperature, pressure and surface energetics, molecular hydrogen can physisorb or chemisorb on the surface. If the intersection of the molecular H_2 potential energy curve with that of atomic hydrogen is above zero, there will be an activation energy barrier (E_A) for hydrogen dissociation (the required work to split hydrogen molecules into atoms). If this

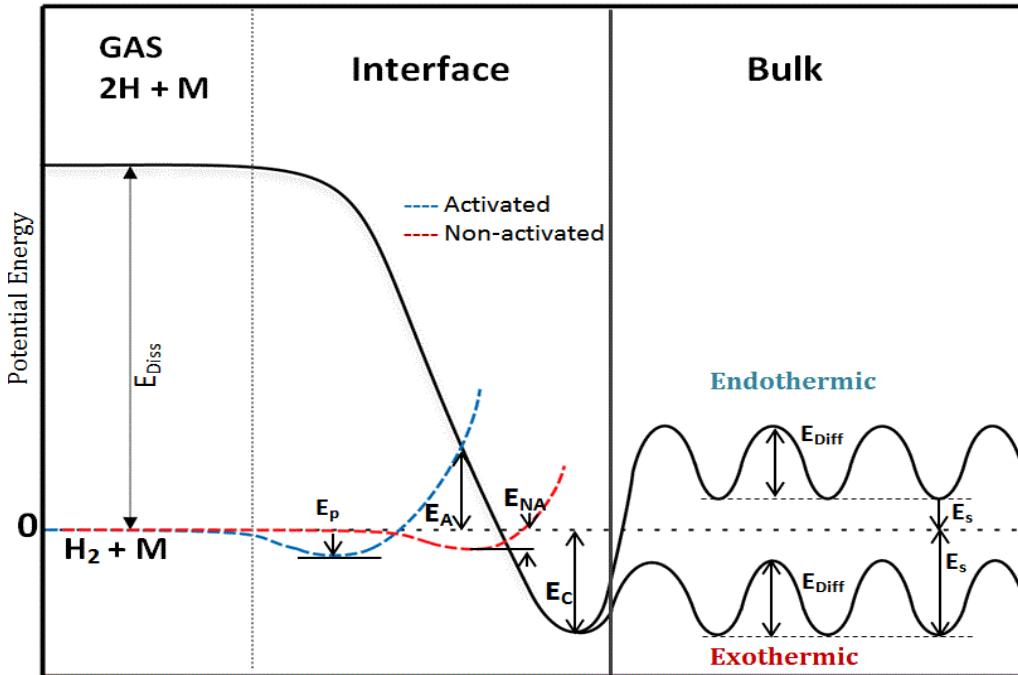


Figure 1-2 The potential energy curve demonstrates corresponding energy barriers for interaction of hydrogen with two different metals, one with positive (Endothermic) and the other with negative (exothermic) heat of solution ΔH_{sol} [22].

activation energy is not available, molecular hydrogen physisorbs on the surface through weak bonds in the form of van der Waals forces or electrostatic attraction with energy levels ranging between 1 and 5 $Kj.mol^{-1}$ (E_p) [16]. The coverage ratio Θ which is defined as the number of physisorbed hydrogen molecules divided by the

number of the adsorption sites is related to temperature (T), pressure (P), binding energy (ϵ) and rate constant (K_L) as follows;

$$\Theta = \frac{K_L P}{K_L P + 1} \quad 1-1$$

$$K_L \sim T^{-0.5} \exp\left(\frac{-\epsilon}{K_B T}\right) \quad 1-2$$

According to above equation, for carbon-based materials with high surface area, enormous interaction is achieved when cryogenic temperatures are applied.

In case where the intersection occurs below zero line, the molecular hydrogen and the host interact chemically and form a new compound. This process is called chemisorption which has binding energy level well above 50 KJ.mol⁻¹ [Ec in figure 1-2]. The formation of chemical bonding requires firstly splitting of molecular hydrogen and secondly electron transfer between the metal and hydrogen. If the potential energy of hydrogen in bulk stays below zero line, the solid solution is said to be exothermic; whereas the solid solution is endothermic if the potential energy of hydrogen in metal is higher than that of molecular hydrogen.

Some transition metals possess d-orbitals which can interact with the hydrogen antibonding orbital to facilitate the dissociation process. Examples are Ni and Pd with low dissociation energy barrier. However, for some metals such as magnesium, this energy barrier is high on the order of 432 KJ.mol⁻¹ [17].

In cases where a surface reaction is the rate limiting step, the kinetic model which is applied is as follows:

$$f=kt$$

f is the fraction of reaction completed and k is a rate constant and t is time.

1.3.2 Penetration and diffusion of hydrogen inside metallic matrix

If a hydrogen molecule can be split on the surface, it diffuses into the metal and is dissolved in the α -phase. Above a specific hydrogen concentration, β -phase nucleates and grows into the metal phase. The energy barriers in this step are associated with energies required for nucleation and diffusion processes. In most cases, the nucleation and growth of hydride phase is modeled by the Johnson-Mehl-Avrami (KML) equation [18]:

$$f=1-\exp [-(kt)^n] \quad 1-4$$

Where f is the fraction of transformation completed, k is the rate constant, n is the Avrami constant giving information about dimensionality of growth and rate limiting step and t is the time.

In general, the reaction rate depends not only on the temperature but also on the pressure

$$K_r=K(P).K(T)=K(P). A \exp \left(\frac{-E_{act}}{kT} \right) \quad 1-5$$

This equation shows an exponential dependency of overall reaction rate (K_r) with temperature. The pressure term, also known as the driving force function has to be

taken into account for determination of activation energy of transformation [19]. For metal/hydride transformation, the pressure term is selected based on the rate-limiting step. Table 1 summarizes the different form of $K(P)$.

Table 1-1 various relationships of pressure term based on different limiting steps

K(P)	Absorption	Desorption
Rate limiting step		
Diffusion	$K(P) = 1 - (P_{eq}/P)^{0.5}$	$K(P) = 1 - (P/P_{eq})^{0.5}$
Phase transformation	$K(P) = \ln (P/P_{eq})$	$K(P) = \ln (P_{eq}/P)$
Adsorption	$K(P) = P - P_{eq}$	$K(P) = P_{eq} - P$

In order to obtain the activation energy E_{act} , after determining the rate limiting step using kinetics models, the $K(T)$ is calculated at different temperatures considering the fact that pressure term ($K(P)$) should be same for all temperatures. Plotting the of rate constant logarithm versus reciprocal temperature (figure 1-3) gives a straight line of which the slope is equal to E_{act}/R .

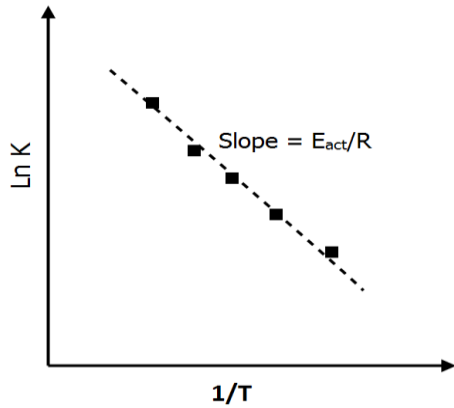


Figure 1-3 Plot of logarithmic rate constant vs reciprocal temperature.

1.3.3 Thermodynamics of metal hydrides formation

The thermodynamics of hydrogen reaction with metal can be depicted in a pressure-composition isotherm. The reaction with hydrogen can be described as follows:

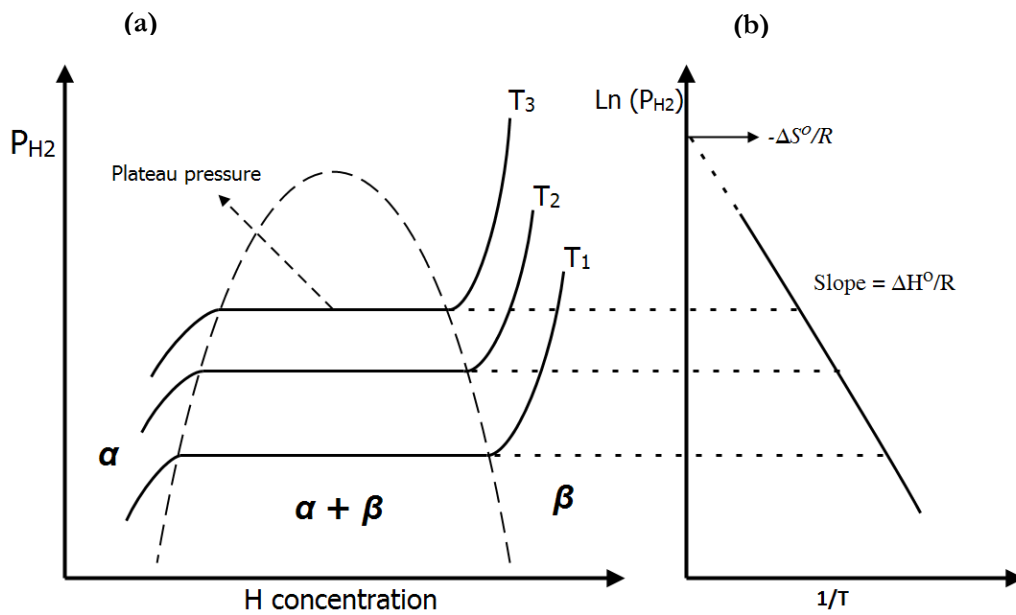


Figure 1-4 Pressure-composition isotherms diagram for a typical Metal-Hydride transformation (a) and corresponding van't Hoff plot (b).

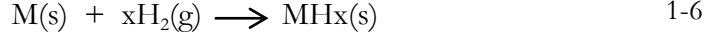


Figure 1-4 depicts a typical pressure-composition isotherm (PCT) curve of metal hydrides. Three distinct regions exist in the diagram. In region 1, the α -phase can dissolve hydrogen up to the solubility limit. Since two phases are in equilibrium, the chemical potential ($\mu_{H_2}^g$) of hydrogen in gas and in solid solution ($\mu_{H_2}^\alpha$) should be equal:

$$\frac{1}{2}\mu_{H_2}^g(P,T) = \mu_{H_2}^\alpha(P,T,x) \quad 1-7$$

The chemical potential of an ideal gas using statistical thermodynamics calculations is:

$$\mu_{H_2}(P,T) = kT \ln\left(\frac{P}{P^o}\right) - E_d \quad 1-8$$

$$P^o = \frac{8(\pi k_B T)^{\frac{7}{2}} M^{\frac{5}{2}} r_o^2}{h^5} \quad 1-9$$

Where E_d is the dissociation energy of hydrogen molecule, k_B is the Boltzmann constant, T is temperature in kelvin, M is the mass of H_2 , r_o is the atomic distance in H_2 molecule and h is Planck's constant. P^o is the pressure at room temperature.

The Gibbs free energy term ($G_{H_2}^\alpha$) for hydrogen atoms in solid solution of α -phase can be expressed as:

$$G_{H_2}^\alpha = H_{H_2}^\alpha - TS_{H_2}^\alpha \quad 1-10$$

The entropy part can be divided to excess entropy and partial ideal configurational entropy (S^i)

$$S = S^{ex} + S^i \quad 1-11$$

Considering b as the number of interstitial sites and x as the number of hydrogen atoms in these sites, the configuration entropy can be written

$$S^i = -k \ln \left(\frac{b!}{x!(b-x)!} \right) \quad 1-12$$

Applying Sterling's approximation we have

$$S^i = kb \ln \left(\frac{b}{b-x} \right) - kx \ln \left(\frac{x}{b-x} \right) \quad 1-13$$

Therefore we have

$$G_H = H_H - TS_H^{ex} + kbT \ln \left(\frac{b}{b-x} \right) - kxT \ln \left(\frac{x}{b-x} \right) \quad 1-14$$

Thus the chemical potential of hydrogen atom will be,

$$\mu_H(P, T, x) = \frac{\delta G_H}{\delta x} = h_H - T s_H^{ex} + kT \ln \left(\frac{x}{b-x} \right) \quad 1-15$$

Where h_H is the partial enthalpy and s_H^{ex} is the non-configurational part of the partial entropy of hydrogen in α -phase. Assuming low concentration of hydrogen i.e. $x \ll b$

$$\ln \left(\frac{x}{b-x} \right) = \ln x - \ln b \quad 1-16$$

Finally, equating eq. 8 and eq. 15 gives

$$\frac{1}{2}k_B T \ln \frac{p}{p^o} - \frac{1}{2}E_d = h_H - T s_H^{ex} + k_B T \ln x - k_B T \ln b \quad 1-17$$

This is Sievert's law [20] for dilute solution which can be written in the following form:

$$x = K \sqrt{\frac{p}{p^o}} \quad 1-18$$

And K is

$$K = \exp\left(\frac{k_B T \ln b + T s_H^{ex} - h_H - \frac{1}{2}E_d}{k_B T}\right) \quad 1-19$$

The solubility limit (x) of hydrogen can vary in a specific system at a fixed temperature due to microstructural changes effecting b, s_H^{ex} and h_H parameters. It has been shown for palladium that a nanocrystalline structure can dissolve hydrogen more than polycrystalline Pd [21]. This behavior is attributed to higher density of grain boundaries in nanocrystalline palladium.

Above the solubility limit, it is thermodynamically favourable for the formation of a second phase (β -phase) which in most cases has different structure than that of host metal. This transition is accompanied with a change in crystalline structure and volume expansion. The volume expansion upon hydriding results in a transform of metal to micro size powder.

According to Gibbs phase rule, in the second region in figure 1-4a, when three phases (i.e. hydrogen gas, metal and metal hydride) are in equilibrium the degree of freedom is one:

$$f = C - P + 2$$

$$f = 2 - 3 + 2 = 1 \quad 1-21$$

Note that C is the number of components and P is the number of phases. A Degree of freedom one at this region requires that pressure and temperature is related. This relation can be found through following calculations:

For reaction 1-6 we have

$$\Delta G = \Delta G^\circ + RT \ln \left(\frac{a_{\text{MgH}_2} P^\circ}{a_{\text{Mg}} P_{\text{H}_2}} \right) \quad 1-22$$

Activity of every pure phase is equal one. Knowing at equilibrium $\Delta G = 0$, thus,

$$RT \ln (P_{\text{H}_2}) = \Delta G^\circ \quad 1-23$$

$$RT \ln (P_{\text{H}_2}) = \Delta H^\circ - T\Delta S^\circ \quad 1-24$$

$$\ln (P_{\text{H}_2}) = \frac{\Delta H^\circ}{RT} - \frac{\Delta S^\circ}{R} \quad 1-25$$

This is the known as the van't Hoff equation, which shows the relation of equilibrium pressure and temperature. ΔH represents the heat which is absorbed or released during reaction. For most of metal hydrides it is negative, which points out that heat is released at the price of metal-hydrogen bond formation. The main constitutive part in ΔS comes from the entropy reduction in hydrogen when gaseous hydrogen is converted to chemisorbed H at the surface ($-130 \text{ KJ}\cdot\text{mol}^{-1}\text{K}^{-1}$) [22]. Plotting $\ln (P_{\text{H}_2})$ versus reciprocal temperature results in a linear plot of which the

slope gives the enthalpy and the x intersect gives the entropy of hydride formation. A typical van't Hoff plot is shown in figure 1-4b.

As mentioned above, the main force which drives the hydriding transition is the Gibbs free energy. However, there is always a kinetics barrier for the hydriding transformation. Figure 1-5 schematically demonstrates the kinetic energy barriers (activation energy) involved in the transformation and the difference between enthalpy of metal and metal hydride. Studies have shown that size reduction and addition of alloying elements can be utilized to decrease both kinetic energy barrier and bonding energy of metal-hydrogen [22, 23, 24, 25].

One way to destabilize a hydride is to alloy a metal with a strong hydrogen bond affinity with element such as Ni, Pd and Si. By the formation of an intermetallic hydride, the heat of formation is reduced while at the same time there is a considerable loss in capacity and the kinetics become slow in most cases. Another route to the destabilization of hydride is the utilization of nanotechnology. Nanomaterials exhibit properties different from those of bulk. Because of high surface area to volume ratio, the contribution of the surface to total free Gibbs energy of system is non-negligible in nanomaterials. A simple modified van't Hoff equation for nano-structure metal can be expressed as follows:

$$\ln \frac{P_{\text{eq, nano}}}{P_{\text{H}_2}} = \frac{1}{RT} \left(\Delta H^\circ + \left(\frac{V_M Y_M}{r_M} - \frac{V_{\text{MH}_2} Y_M}{r_{\text{MH}_2}} \right) \right) - \frac{\Delta S^\circ}{R} \quad 1-26$$

Where γ is the surface energy, r is the radius of metal/hydride particle and V is the molar volume. When the contribution from size effect become negative enough, it reduces the enthalpy term and hydride is destabilized. Theoretical calculations predict that particles of 2 nm size have enthalpy which is much lower than that of the bulk version of same material [26, 27].

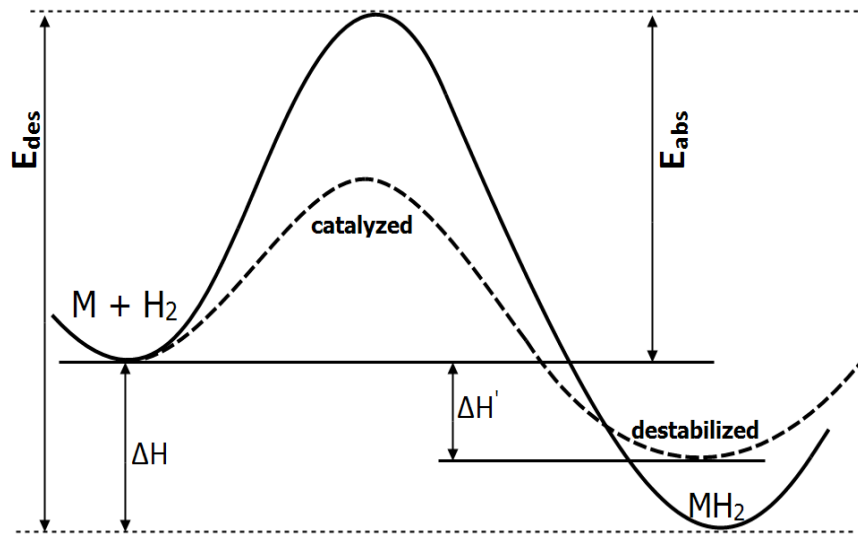


Figure 1-5 Energy diagram for (de)hydrogenation of metal (metal hydride). When catalyzed, the energy barrier decreases for both absorption and desorption. When destabilized, the temperature can be reduced for desorption due to less stable bonding between metal and hydrogen.

1.4 Magnesium Hydride

When considering a medium for hydrogen storage, it is important to take into account the capacity of that medium. Magnesium with 7.6 wt.% hydrogen capacity has attracted much attention [17]. However, slow kinetics and high stability of the

hydride formed are main issues for magnesium. Magnesium has hexagonal structure (194 space group P63/mmc, $a=3.2089 \text{ \AA}$, $c=5.2101 \text{ \AA}$). Upon hydrogenation it transforms to tetragonal rutile-type magnesium hydride (136 space group P42/mnm, $a=4.5147 \text{ \AA}$, $c=3.0193 \text{ \AA}$). MgH_2 has an enthalpy on the order of 74.7 KJ.mol^{-1} . This is relatively a high value and makes it impossible for hydrogen to be released at low temperature and ambient pressure. In fact, MgH_2 transforms to magnesium at temperature around $300 \text{ }^\circ\text{C}$ for powder samples.

Several approaches have been proposed to improve the poor kinetics and thermodynamics of Mg-based hydrogen storage systems. One can obtain faster kinetic rates by the reduction of particle and grains size. Size reduction can shorten diffusion distances and higher surface area can change the surface energy and hydrogen sorption properties. It has been reported that the desorption temperature of as-received MgH_2 powder can be reduced by reducing the size of Mg powder to the nano-scale [17]. The most common and practical method for the implementation of such an idea is through ball milling of powder samples. Ball milling not only refines the microstructure and increases surface area, but also it creates defects such twins and dislocations in microstructure which have been identified as effective routes for tuning sorption properties [28, 29]. However, the major issue is that all above affects will increase the free Gibbs energy and drive recrystallization. The driven coalescing and grain growth result in loss of improved properties. To overcome this obstacle, magnesium hydride is mixed with additives, especially transition metals, which help ease the dissociation of hydrogen, improve the

cyclability of Mg powder and stabilize the tuned microstructure during cycling. Nonetheless, maintaining reduced particle size during cycling and obtaining good dispersion of catalyst are key challenges to achieve good performance through ball milling.

The use of Mg-based thin films for hydrogen storage has emerged as an alternative to tune properties of magnesium for hydrogen storage [30, 31, 32, 33]. Thin films are attractive due to their higher surface area and better heat management than bulk samples. The main concern with thin films is that they must be deposited on to a substrate and even though significant properties enhancement are achieved, the final weight is the summation of both the substrate and the storage material. In addition, the microstructure in thin film might not be stable as it can deteriorate during cycling [34].

Magnesium-3rd transition metal thin films have been investigated in last decades. Ti, Fe, V and Nb are alloying elements that have been mostly used for tailoring properties of Mg-based thin films [32, 33, 34, 37, 38, 39]. Griessen et.al has been studying hydrogen sorption properties of Mg-Ti alloy thin films at low temperatures. Due to formation of a metastable face-centered cubic phase in Mg-Ti-H thin films compared with rutile-type structure in Mg, the kinetics significantly improved [40]. However, upon cycling at higher temperature around 200 °C , the metastable hydride phase decomposes to a binary hydride phase with a noticeable loss in capacity and degradation in kinetics [35]. In his research on Nb-doped magnesium, Miotello found that a good distribution of Nb in a metal matrix results in a considerable

reduction in activation energy of sorption and they suggested that the rate limiting step in desorption reaction changed from surface dissociation for Mg to diffusion-controlled for catalyzed Mg [37]. The activation energy for catalyzed Mg was 51 kJ/mol H₂ compared to pure Mg, which was reported to be 141 kJ/mol H₂. It has been shown that ternary alloy systems behave significantly better in term of cyclability and accelerated kinetics than binary alloys [35, 41]. In this regard, Mg-Fe-Ti, Mg-Al-Ti, Mg-Fe-Zr display better performance than binary systems, such as Mg-Fe, Mg-Al, Mg-Ti, Mg-Zr.

Magnesium-based multilayer thin films are subject to extensive research due to their unique structural properties. When capped with Pd, Mg film shows significant thermodynamics enhancement due to the elastic strain interaction at the interface between Mg and Pd [42, 43]. The material can absorb/desorb hydrogen at 100 °C, demonstrating substantial reduction in sorption temperature compared to pure Mg. As for the Mg-Ti alloys, studies have been done on the hydrogen storage properties of Mg/Ti multilayer thin films [33, 43, 44]. The catalytic effect of Ti layers was found to be responsible for the improved kinetics behavior while those layers forming alloys with Mg such as Ni and Pd have an effect on the thermodynamics property of films.

1.5 Scope of this project

Thin film materials can be used to explore the effect of catalyst in the form of dispersed particles and layered structure in tuning sorption properties of magnesium.

Multilayered structure of magnesium confined between secondary layers enables us to reduce size of magnesium and control it as a key role in long-term performance of fine structure materials. In addition, one is able to tune the thermodynamics of Mg-based material by introducing new interface energy which can change the energy of Mg/MgH₂ interface and contribute to total energy of hydriding reaction. To achieve the mentioned enhancement, multilayer Mg/AlTi thin films were synthesized to:

1. Reduce the size of Mg particles and prevent its grain growth during cycling
2. Increase the effect of surface energies and their contribution to sorption properties of magnesium

The addition of Al to magnesium-titanium system has been reported to significantly improve the kinetics behavior [45]. While it shows significant enhancement in kinetics properties, the enthalpy of system is similar to pure Mg and remains unchanged. By sandwiching Mg between AlTi layers, we first investigate the possibility of increasing the cycle-life of multilayer structure without kinetics degradation. Secondly, we explore the effect of increasing Mg/AlTi interface energy to lower the energy bond interaction between Mg and H, i.e. reducing the heat of formation.

1.6 References

- [1] V. A. Yartys and M. V. Lototsky, "An Overview of Hydrogen Storage Methods," in Hydrogen Materials Science and Chemistry of Carbon Nanomaterials,

vol. 172, T. N. Veziroglu, S. Zaginaichenko, D. V. Schur, B. Baranowski, A. P. Shpak, and V. V. Skorokhod, Eds. Springer Netherlands, 2005, pp. 75–104.

[2] M. Conte, P. . Prosini, and S. Passerini, “Overview of energy/hydrogen storage: state-of-the-art of the technologies and prospects for nanomaterials,” *Materials Science and Engineering: B*, vol. 108, no. 1–2, pp. 2–8, Apr. 2004.

[3] A. Züttel, A. Remhof, A. Borgschulte, and O. Friedrichs, “Hydrogen: the future energy carrier,” *Phil. Trans. R. Soc. A*, vol. 368, no. 1923, pp. 3329–3342, Jul. 2010.

[4] D. H. Bradhurst, P. M. Heuer, and G. Z. A. Stolarski, “Hydrogen Production and Storage,” Feb. 1981.

[5] A. Züttel, “Hydrogen storage methods,” *Naturwissenschaften*, vol. 91, no. 4, pp. 157–172, 2004.

[6] L. Zhou, “Progress and problems in hydrogen storage methods,” *Renewable and Sustainable Energy Reviews*, vol. 9, no. 4, pp. 395–408, Aug. 2005.

[7] D. Mori and K. Hirose, “Recent challenges of hydrogen storage technologies for fuel cell vehicles,” *International Journal of Hydrogen Energy*, vol. 34, no. 10, pp. 4569–4574, May 2009.

[8] A. Züttel, “Materials for hydrogen storage,” *Materials Today*, vol. 6, no. 9, p. 24–33, Sep. 2003.

[9] I. Cumalioglu, A. Ertas, Y. Ma, and T. Maxwell, “State of the Art : Hydrogen storage,” *Journal of fuel cell science and technology*, vol. 5, no. 3.

[10] G. Liang, J. Huot, S. Boily, A. Van Neste, and R. Schulz, “Catalytic effect of transition metals on hydrogen sorption in nanocrystalline ball milled MgH₂-Tm (Tm=Ti, V, Mn, Fe and Ni) systems,” *Journal of Alloys and Compounds*, vol. 292, no. 1–2, pp. 247–252, Nov. 1999.

[11] J.-L. Bobet, E. Akiba, and B. Darriet, “Study of Mg-M (M=Co, Ni and Fe) mixture elaborated by reactive mechanical alloying: hydrogen sorption properties,” *International Journal of Hydrogen Energy*, vol. 26, no. 5, pp. 493–501, May 2001.

[12] J. J. Reilly and R. H. Wiswall, “Reaction of hydrogen with alloys of magnesium and nickel and the formation of Mg₂NiH₄,” *Inorg. Chem.*, vol. 7, no. 11, pp. 2254–2256, 1968.

- [13] J. J. Vajo, F. Mertens, C. C. Ahn, Bowman, and B. Fultz, "Altering Hydrogen Storage Properties by Hydride Destabilization through Alloy Formation: LiH and MgH₂ Destabilized with Si," *J. Phys. Chem. B*, vol. 108, no. 37, pp. 13977–13983, 2004.
- [14] J. J. Vajo and G. L. Olson, "Hydrogen storage in destabilized chemical systems," *Scripta Materialia*, vol. 56, no. 10, pp. 829–834, May 2007.
- [15] J. E. Lennard-Jones, "Processes of adsorption and diffusion on solid surfaces," *Transactions of the Faraday Society*, vol. 28, p. 333, 1932.
- [16] A. Centrone, L. Brambilla, and G. Zerbi, "Adsorption of H₂ on carbon-based materials: A Raman spectroscopy study," *Phys. Rev. B*, vol. 71, no. 24, p. 245406, Jun. 2005.
- [17] K.-F. Aguey-Zinsou and J.-R. Ares-Fernández, "Hydrogen in magnesium: new perspectives toward functional stores," *Energy & Environmental Science*, vol. 3, no. 5, p. 526, 2010.
- [18] E. Pineda and D. Crespo, "Microstructure development in Kolmogorov, Johnson-Mehl, and Avrami nucleation and growth kinetics," *Phys. Rev. B*, vol. 60, no. 5, pp. 3104–3112, 1999.
- [19] B. Zahiri, M. Danaie, X. Tan, B. S. Amirkhiz, G. A. Botton, and D. Mitlin, "Stable Hydrogen Storage Cycling in Magnesium Hydride, in the Range of Room Temperature to 300 °C, Achieved Using a New Bimetallic Cr-V Nanoscale Catalyst," *J. Phys. Chem. C*, vol. 116, no. 4, pp. 3188–3199, 2011.
- [20] C. K. Gupta, "Front Matter," in *Chemical Metallurgy*, Wiley-VCH Verlag GmbH & Co. KGaA, 2004, p. i–xx.
- [21] A. Pundt and R. Kirchheim, "Hydrogen in Metals: Microstructural Aspects," *Annual Review of Materials Research*, vol. 36, no. 1, pp. 555–608, 2006.
- [22] V. Bérubé, G. Radtke, M. Dresselhaus, and G. Chen, "Size effects on the hydrogen storage properties of nanostructured metal hydrides: A review," *International Journal of Energy Research*, vol. 31, no. 6–7, pp. 637–663, 2007.
- [23] N. Hanada, T. Ichikawa, and H. Fujii, "Catalytic Effect of Nanoparticle 3d-Transition Metals on Hydrogen Storage Properties in Magnesium Hydride MgH₂ Prepared by Mechanical Milling," *J. Phys. Chem. B*, vol. 109, no. 15, pp. 7188–7194, 2005.

- [24] R. L. Holtz and M. A. Imam, "Hydrogen storage characteristics of ball-milled magnesium-nickel and magnesium-iron alloys," *Journal of Materials Science*, vol. 34, no. 11, pp. 2655–2663, 1999.
- [25] R. Schulz, J. Huot, G. Liang, S. Boily, G. Lalande, M. . Denis, and J. . Dodelet, "Recent developments in the applications of nanocrystalline materials to hydrogen technologies," *Materials Science and Engineering: A*, vol. 267, no. 2, pp. 240–245, Jul. 1999.
- [26] R. W. P. Wagemans, J. H. van Lenthe, P. E. de Jongh, A. J. van Dillen, and K. P. de Jong, "Hydrogen Storage in Magnesium Clusters: Quantum Chemical Study," *J. Am. Chem. Soc.*, vol. 127, no. 47, pp. 16675–16680, 2005.
- [27] L. Li, B. Peng, W. Ji, and J. Chen, "Studies on the Hydrogen Storage of Magnesium Nanowires by Density Functional Theory," *J. Phys. Chem. C*, vol. 113, no. 7, pp. 3007–3013, 2009.
- [28] B. S. Amirkhiz, M. Danaie, and D. Mitlin, "The influence of SWCNT–metallic nanoparticle mixtures on the desorption properties of milled MgH₂ powders," *Nanotechnology*, vol. 20, no. 20, p. 204016, May 2009.
- [29] M. Danaie, S. X. Tao, P. Kalisvaart, and D. Mitlin, "Analysis of deformation twins and the partially dehydrogenated microstructure in nanocrystalline magnesium hydride (MgH₂) powder," *Acta Materialia*, vol. 58, no. 8, pp. 3162–3172, May 2010.
- [30] H. Wenzl, K.-H. Klatt, P. Meuffels, and K. Papathanassopoulos, "Hydrogen storage in thin film metal hydrides," *Journal of the Less Common Metals*, vol. 89, no. 2, pp. 489–494, Feb. 1983.
- [31] I. P. Jain, Y. K. Vijay, L. K. Malhotra, and K. S. Uppadhyay, "Hydrogen storage in thin film metal hydride—a review," *International Journal of Hydrogen Energy*, vol. 13, no. 1, pp. 15–23, 1988.
- [32] P. Vermeulen, R. A. H. Niessen, and P. H. L. Notten, "Hydrogen storage in metastable Mg_yTi(1 – y) thin films," *Electrochemistry Communications*, vol. 8, no. 1, pp. 27–32, Jan. 2006.
- [33] A. Baldi, G. K. Pálsson, M. Gonzalez-Silveira, H. Schreuders, M. Slaman, J. H. Rector, G. Krishnan, B. J. Kooi, G. S. Walker, M. W. Fay, B. Hjörvarsson, R. J. Wijngaarden, B. Dam, and R. Griessen, "Mg/Ti multilayers: Structural and hydrogen absorption properties," *Phys. Rev. B*, vol. 81, no. 22, p. 224203, Jun. 2010.

- [34] A. Remhof and A. Borgschulte, "Thin-Film Metal Hydrides," *ChemPhysChem*, vol. 9, no. 17, pp. 2440–2455, 2008.
- [35] W. P. Kalisvaart, C. T. Harrower, J. Haagsma, B. Zahiri, E. J. Lubber, C. Ophus, E. Poirier, H. Fritzsche, and D. Mitlin, "Hydrogen storage in binary and ternary Mg-based alloys: A comprehensive experimental study," *International Journal of Hydrogen Energy*, vol. 35, no. 5, pp. 2091–2103, Mar. 2010.
- [36] P. Mosaner, N. Bazzanella, M. Bonelli, R. Checchetto, and A. Miotello, "Mg:Nb films produced by pulsed laser deposition for hydrogen storage," *Materials Science and Engineering: B*, vol. 108, no. 1–2, pp. 33–37, Apr. 2004.
- [37] N. Bazzanella, R. Checchetto, and A. Miotello, "Catalytic effect on hydrogen desorption in Nb-doped microcrystalline MgH_2 ," *Applied Physics Letters*, vol. 85, no. 22, pp. 5212–5214, Nov. 2004.
- [38] B. Zahiri, C. T. Harrower, B. Shalchi Amirkhiz, and D. Mitlin, "Rapid and reversible hydrogen sorption in Mg–Fe–Ti thin films," *Applied Physics Letters*, vol. 95, no. 10, pp. 103114–103114–3, Sep. 2009.
- [39] M. Gonzalez-Silveira, R. Gremaud, A. Baldi, H. Schreuders, B. Dam, and R. Griessen, "Effect of H-induced microstructural changes on pressure-optical transmission isotherms for Mg–V thin films," *International Journal of Hydrogen Energy*, vol. 35, no. 13, pp. 6959–6970, Jul. 2010.
- [40] A. Baldi, R. Gremaud, D. M. Borsa, C. P. Baldé, A. M. J. van der Eerden, G. L. Kruijtzter, P. E. de Jongh, B. Dam, and R. Griessen, "Nanoscale composition modulations in $Mg_yTi_{1-y}H_x$ thin film alloys for hydrogen storage," *International Journal of Hydrogen Energy*, vol. 34, no. 3, pp. 1450–1457, Feb. 2009.
- [41] N. Bazzanella, R. Checchetto, and A. Miotello, "Catalytic effect of mixed Zr–Fe additives on the hydrogen desorption kinetics of MgH_2 ," *Applied Physics Letters*, vol. 92, no. 5, pp. 051910–051910–3, Feb. 2008.
- [42] K. Higuchi, K. Yamamoto, H. Kajioaka, K. Toiyama, M. Honda, S. Orimo, and H. Fujii, "Remarkable hydrogen storage properties in three-layered Pd/Mg/Pd thin films," *Journal of Alloys and Compounds*, vol. 330–332, no. 0, pp. 526–530, Jan. 2002.
- [43] A. Baldi, M. Gonzalez-Silveira, V. Palmisano, B. Dam, and R. Griessen, "Destabilization of the Mg–H System through Elastic Constraints," *Phys. Rev. Lett.*, vol. 102, no. 22, p. 226102, Jun. 2009.

[44] L. P. A. Mooij, A. Baldi, C. Boelsma, K. Shen, M. Wagemaker, Y. Pivak, H. Schreuders, R. Griessen, and B. Dam, “Interface Energy Controlled Thermodynamics of Nanoscale Metal Hydrides,” *Advanced Energy Materials*, vol. 1, no. 5, pp. 754–758, 2011.

[45] P. Vermeulen, E. F. M. J. van Thiel, and P. H. L. Notten, “Ternary MgTiX-Alloys: A Promising Route towards Low-Temperature, High-Capacity, Hydrogen-Storage Materials,” *Chemistry – A European Journal*, vol. 13, no. 35, pp. 9892–9898, 2007.

2 Microstructural evolution during low temperature sorption cycling of Mg-AlTi multilayer nanocomposites

A version of this chapter has been published in: Zahiri R, Zahiri B, Kubis A, Kalisvaart P, Amirkhiz B, Mitlin D. International Journal of Hydrogen Energy 2012; 37(5): 4215–4226.

2.1 Introduction

Magnesium with a high gravimetric capacity (7.6 wt %) has been considered as a strong candidate for hydrogen storage. However, because of the sluggish sorption kinetics and high thermodynamic stability of magnesium hydride, high temperatures of around 573 K are needed for sorption of magnesium (hydride). Attempts to alter the thermodynamics of magnesium hydride by forming intermetallic compounds with lower enthalpy of hydride formation with elements such as Ni, Cu, Al and Si [1, 2, 3, 4, 5, 6], have not resulted in any viable way to produce large quantities of a practical hydrogen storage material. As a consequence, most research efforts have been directed at improving the sorption kinetics of magnesium hydride. Transition metals in particular have been intensively studied theoretically and experimentally as suitable catalysts for sorption of magnesium (hydride) [7, 8, 9, 10, 11, 12, 13, 14]. The use of carbon materials in combination with transition metals toward a better

dispersion of catalyst along with controlling the size of the particles and the grains has been proposed [15, 16]. Most of these studies in enhancing the sorption kinetics of magnesium have been aimed at reducing the particle size or grain size and incorporating well dispersed catalyst distribution using ball milling technique. In practice, the enhancement achieved through ball milling can be annealed out during sorption cycling [14].

Use of bi-metallic catalysts has been introduced, as metallic additions can form intermetallics during sorption cycling and improve the kinetics via catalysis or in a synergetic way, they act as both catalyst and size control agent [17, 18, 19, 20, 21]. In these works, the most important factors in the stabilization of the kinetics were the prevention of sintering of the magnesium particles and keeping the high free surface area accessible to hydrogen gas for rapid (de)-hydrogenation; and also maintain a uniform dispersion of fine catalyst particles in Mg matrix. However, the challenge to make a Mg-based composite which is catalytically active and stable over many cycles, have a high surface area and is resistance against sintering and agglomeration still remains.

Layered structures, where the catalyst layers can at the same time act as a diffusion barrier against sintering of Mg while simultaneously catalyzing the dissociation of hydrogen are proposed. Mg-based materials with layered morphologies can be produced by cold-rolling techniques [22, 23, 24, 25, 26], sputtering [27, 28], pulsed laser deposition [29] or thermal evaporation and electron gun evaporation [30]. By arranging the Mg and catalyst in a layered structure, the catalyst layers can prevent

sintering of Mg while simultaneously catalyzing the dissociation of hydrogen. In order to preserve the layered structure, the catalyst phase must be chosen from those metals which form no intermetallic compound with Mg [27]. For instance, Pd has been shown to be a poor choice for Mg/Pd multilayers since it forms Mg_6Pd even at 373K which leads to disintegration of the multilayer composite in first hydrogenation [28]. Moreover, it has recently been reported that by sandwiching nanosized Mg alloys between layers of transition metals or catalysts such as Pd or generally by fabricating nanoconfined hydrides, not only are the kinetics of sorption enhanced, but the thermodynamics of hydride formation may potentially be altered [29, 31, 32, 33, 34, 35].

In this study, we propose Mg- $AlTi$ multilayered structures. Both Al and Ti are widely used to enhance sorption behavior of magnesium hydrogen systems. Kalisvaart et al showed for cosputtered Mg-based thin films, the ternary Mg-Al-Ti system has enhanced performance compared to binary Mg-Ti or Mg-Al in terms of cycling stability and kinetics [36, 37]. Since Al reacts more strongly with Ti than Mg, the intermetallic $AlTi$ forms which enhances the kinetic and hydrogen sorption behavior [37]. Employing $AlTi$ layers seems desirable due to good catalyst activity and high mechanical properties rather than individual Ti or Al layers. Moreover, $AlTi$ forms no hydride while it has negligible interaction with hydrogen and thus it has a very low solubility of hydrogen [37]. Thus, $AlTi$ can act as high diffusivity channels for hydrogen while it can hinder the sintering of magnesium when it is used in the form of layers between Mg layers. The kinetics and capacity of the multilayers are studied

as a function of Mg layer thickness, and the evolution of their microstructure is studied by electron microscopy techniques and X-ray diffraction (XRD) in this chapter. The ability of AlTi layers to act as coarsening barriers is evaluated. Furthermore, the effect of addition of Al and Ti to the individual magnesium layers is investigated. It is expected that multilayers consisting of cosputtered Mg-Al-Ti layers sandwiched between AlTi layers show enhanced kinetics and improved cyclability and mechanical stability.

2.2 Experimental techniques

Magnetron sputtering system (AJA International) was used to deposit Mg/AlTi multilayer thin films of 1.5 mm thickness coated with 7.5 nm Pd/Ta bi-layers. Palladium can protect samples from oxidation and catalyze hydrogen dissociation while tantalum suppresses the interdiffusion of magnesium and palladium [38]. All samples were prepared under mean base pressure of approximately 8×10^{-8} bar and argon (purity of 99.999%) pressure of 4 torr and flow rate of 20 sccm. To ease film lift-off after the deposition process, a very thin layer of photoresist is applied on the surface of wafers. To do so, wafers are thoroughly cleaned using a 3:1 mixture of H_2SO_4 and H_2O_2 . Approximately, 5 ml of HPR 504 is poured into the center of wafer and it is spun for 10 seconds at the rate of 500 rpm. After 10 seconds, the rate increases to 4000 rpm for 40 seconds to dry the photoresist. Finally, the wafer is baked for 90 seconds at 120 °C to remove the residual solvent and achieve good adhesion. The final thickness of photoresist is 1.25 μm . Through acetone dissolution

of photoresist for one hour, free standing thin films are achieved which are ready for testing sorption properties.

We made different Mg/AlTi multilayer thin films with the fixed 2 nm AlTi (Al:Ti ratio of 1) layers and different magnesium layers of 10, 20 and 34 nm. In choosing these thicknesses for Mg layers, final capacities and overall compositions were considered. For simplicity we denote samples X/Y name in which X is the thickness of magnesium and Y is the thickness of intermetallic AlTi layers in nm. We prepared one sample with the Mg layers cosputtered with Al and Ti. This sample consisted of cosputtered 20 nm Mg-7% at Al-7% Ti layers and 2 nm AlTi layers which has the same number of layers as 20/2 multilayers and the capacity close to that of 10/2 multilayer. This sample is denoted cosputtered 20/2 multilayer. Sievert's apparatus (HyEnergy LLC. PCTPro 2000) was used to run cyclic kinetic measurements as well as PCT measurements. Test samples mass varied between 10 and 15 mg. Absorption Pressure was 2.5-0.1 bar, while desorption was run under low vacuum in a 1025 ml reservoir. The sorption process was automatically cut when the sorption rate fell below 0.005 wt.%/min. All sorption tests were done at 473 K. For PCT measurements, the pressure-composition isotherms were acquired after the samples were activated.

For X-ray diffraction analysis, we used a Bruker AXS diffractometer (Bruker Discover 8) operating with Cu-K α radiation with wavelength of 1.5405 Å. To determine the grain size, we incorporated integral breath analysis (IBA) in which the following relation is used:

$$\frac{(\delta 2\Theta)^2}{\tan^2 \Theta_o} = \frac{k\lambda}{D \sin \Theta_o \tan \Theta_o} \delta 2\Theta + 16 \epsilon^2$$

While $\delta 2\Theta$ is the integral breath of each peak and Θ_o is the position of peak maximum. The slope of linear fitted curve from the plot of $(\delta 2\Theta)^2/(\tan^2 \Theta_o)$ vs $(\delta 2\Theta)/(\sin \Theta_o \tan \Theta_o)$ being $k\lambda=D$ was used to determine the grain size (D) and microstrain (ϵ). The value of k was assumed as 0.9 for cubic structures and x-ray wavelength (λ) was 1.5406 Å. We performed transmission electron microscopy (TEM) using JEOL 2010 and JEOL 2200FS operating at 200 kV. JEOL 2200FS enabled us to run energy-dispersive X-ray spectroscopy (EDX) elemental mapping in scanning TEM mode (STEM). We used high angle annular dark field (HAADF) imaging to form z-contrast images where heavier atoms of Al and Ti are in contrast with lighter Mg atoms. With the help of focused ion beam (FIB) lift-out technique using a two beam FIB-SEM system (Zeiss NVision 40) we were able to take cross-sectional images of multilayered samples even after cycling. FIB technique was also incorporated to prepare cross sectional TEM ready samples.

2.3 Results

2.3.1 Kinetics

Figures 2-1 and 2-2 depict the absorption and desorption behavior of 10/2 and cosputtered 20/2 multilayer samples up to 250 cycles. An activation period is a common feature of every sample which increases as the thickness of magnesium

layer decreases, that is, when the periodicity increases. In this case, 34/2 multilayer has the lowest activation period in which only 4 cycles were needed to activate the

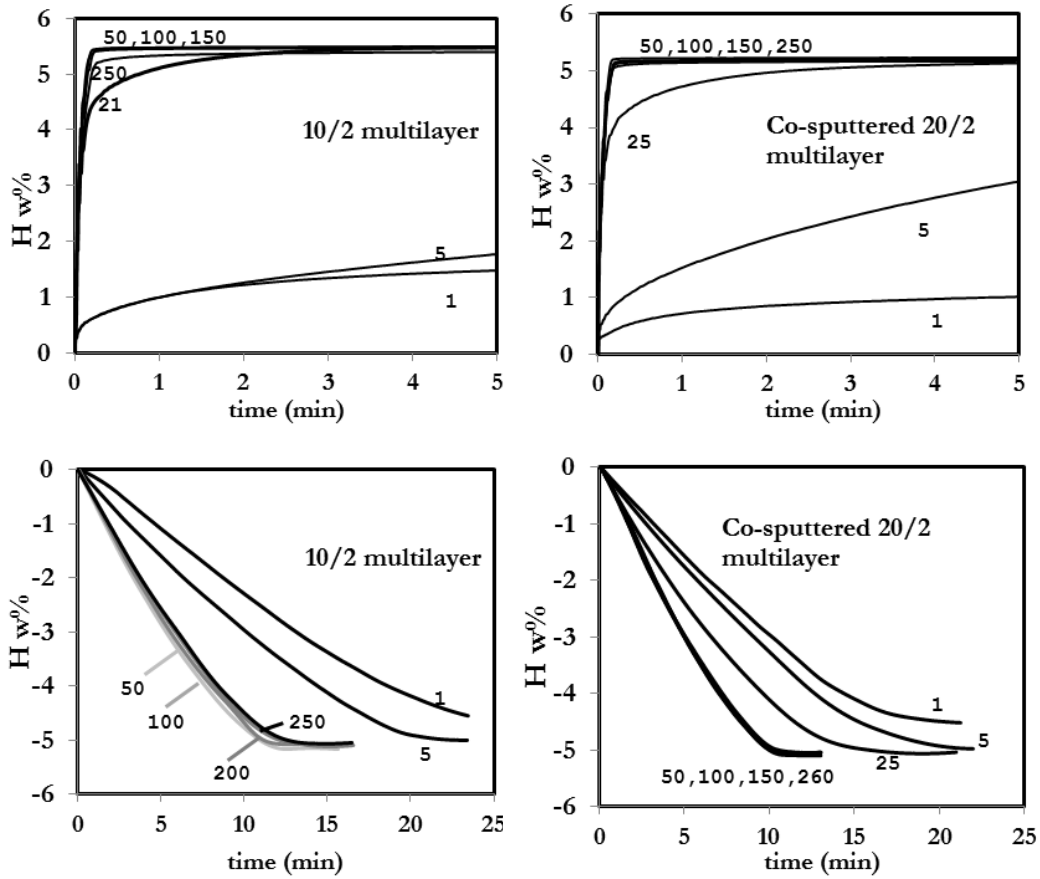


Figure 2-1 Absorption and desorption behavior of 10/2 (A,C), co-sputtered 20/2 (B,D) multilayer samples.

material; albeit the initial cycles during activation period are very slow and more than 1 h is required to obtain fully absorbed material. As shown in the time to 90% capacity as a function of cycling in the inset of figure 2-3A, during activation the kinetics of absorption is very sluggish for all the composites; after activation, it occurs within seconds. As for desorption, as also illustrated in figure 2-3B, it takes approximately 25 min for the samples to desorb in the initial cycles, while after

activation desorption time reduced by a factor of 2 for 10/2 multilayer and 2.5 for co-sputtered 20/2 multilayer to desorb completely.

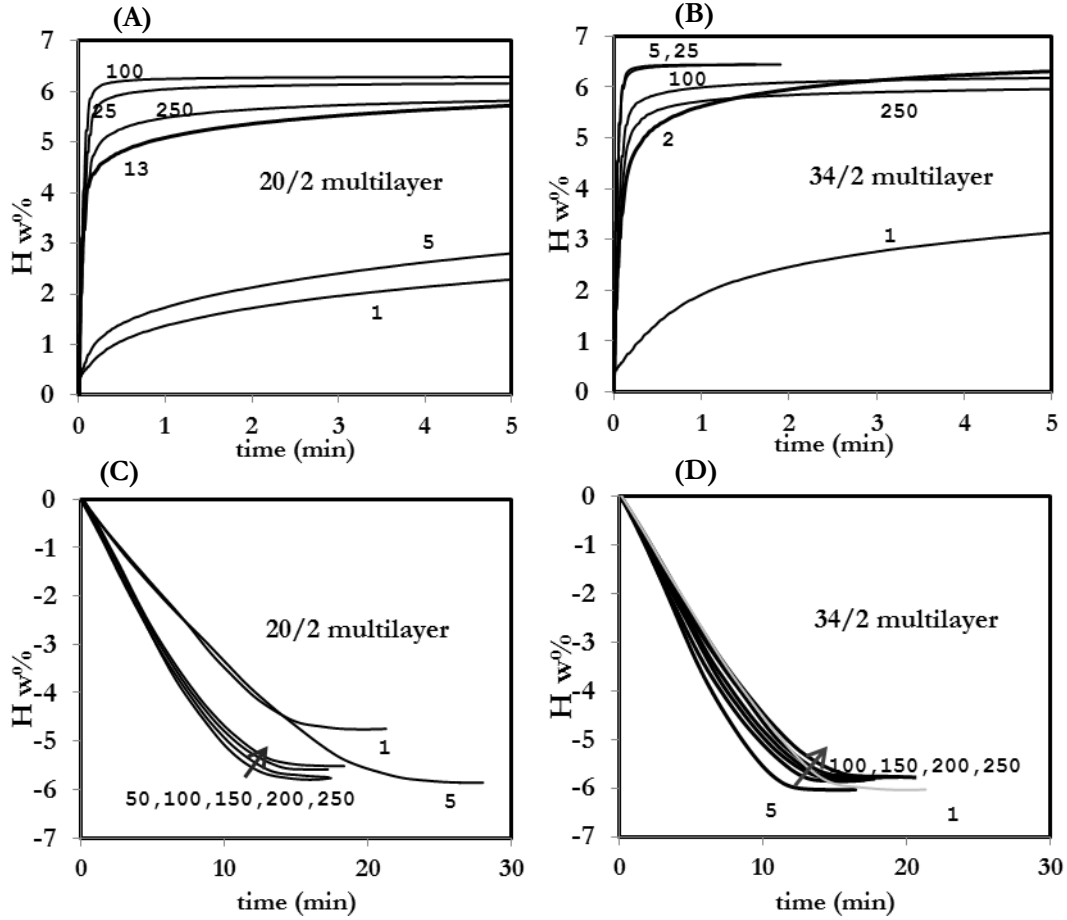


Figure 2-2 Absorption and desorption behavior of 20/2 (A,C) and 34/2 (B,D) multilayer samples.

According to figure 2-3 co-sputtered 20/2 multilayer shows the best cycling performance being stable up to 250 cycles, while the samples with pure magnesium layers tend to degrade slowly after having a stable cycling period. Among samples with pure Mg layers, 10/2 multilayer has comparable behavior to co-sputtered 20/2 multilayer; however, the former starts to degrade eventually which is clearly reflected

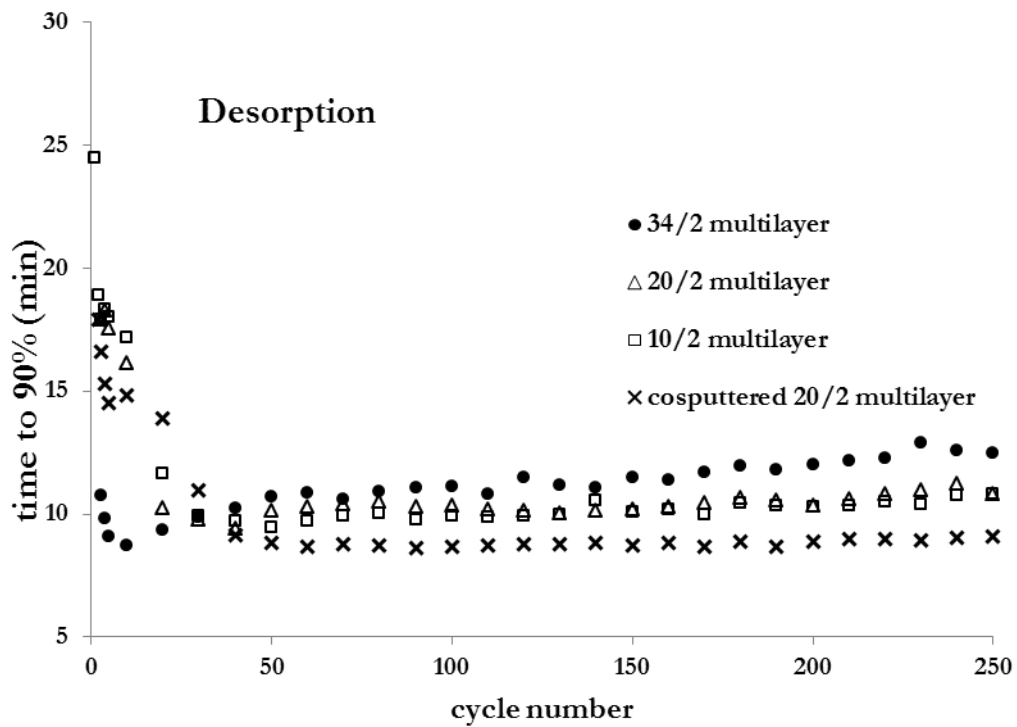
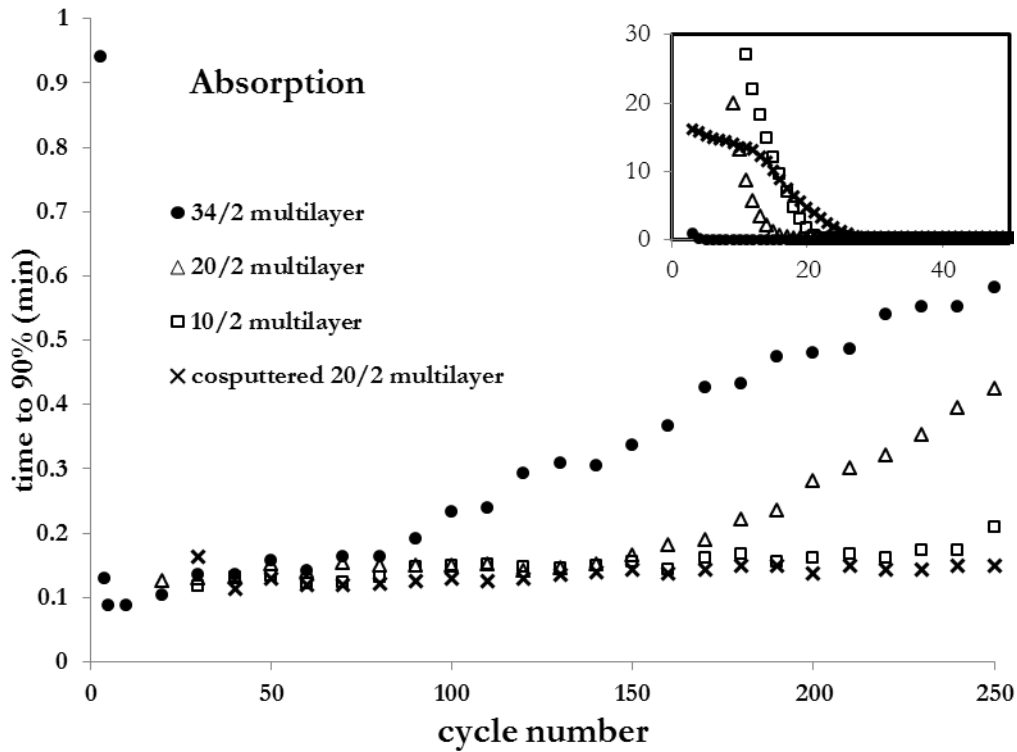


Figure 2-3 The time to reach 90% of average maximum capacity as a function of cycle number for (A) absorption and (B) desorption.

in the absorption curves. Apparently, with increasing the magnesium thickness, the onset for degradation moves toward lower cycle numbers. Comparing the co-sputtered 20/2 to 20/2 multilayer, it appears that co-sputtering of magnesium layers with Al and Ti (Mg-7% Al-7Ti) remarkably enhances the stability of the material. The inset, in the absorption plot, shows the first 40 cycles which points out the remarkably longer activation period for sample with thinner magnesium layers with the thinner magnesium layers with the exception of co-sputtered multilayer which has the longest activation period; although during activation it has faster kinetics.

2.3.2 Thermodynamics

Theoretical work by Wagemans et al. suggests that reducing the particle size of Mg(H₂) to extremely small sizes can change the thermodynamic properties for particles with fewer than 10 Mg atoms [39]. In the present deposition configuration, this theoretical limit corresponds to a layer thickness of approximately 2 nm which is below the dimensions used in the current study. However, studies by Baldi et al. showed destabilization of 20 nm Mg layer sandwiched between Pd and TiH₂ layers [34, 35]. The destabilization effect was attributed to clamping effects at the Mg/Pd interface due to the strong alloying tendency between Mg and Pd. In a more recent work they showed that alloying tendency is not necessary for thermodynamics alteration since for Mg/Ti multilayers, where the Ti layers hydrogenate before Mg, destabilization takes place for an Mg layer thinner than 10 nm [40].

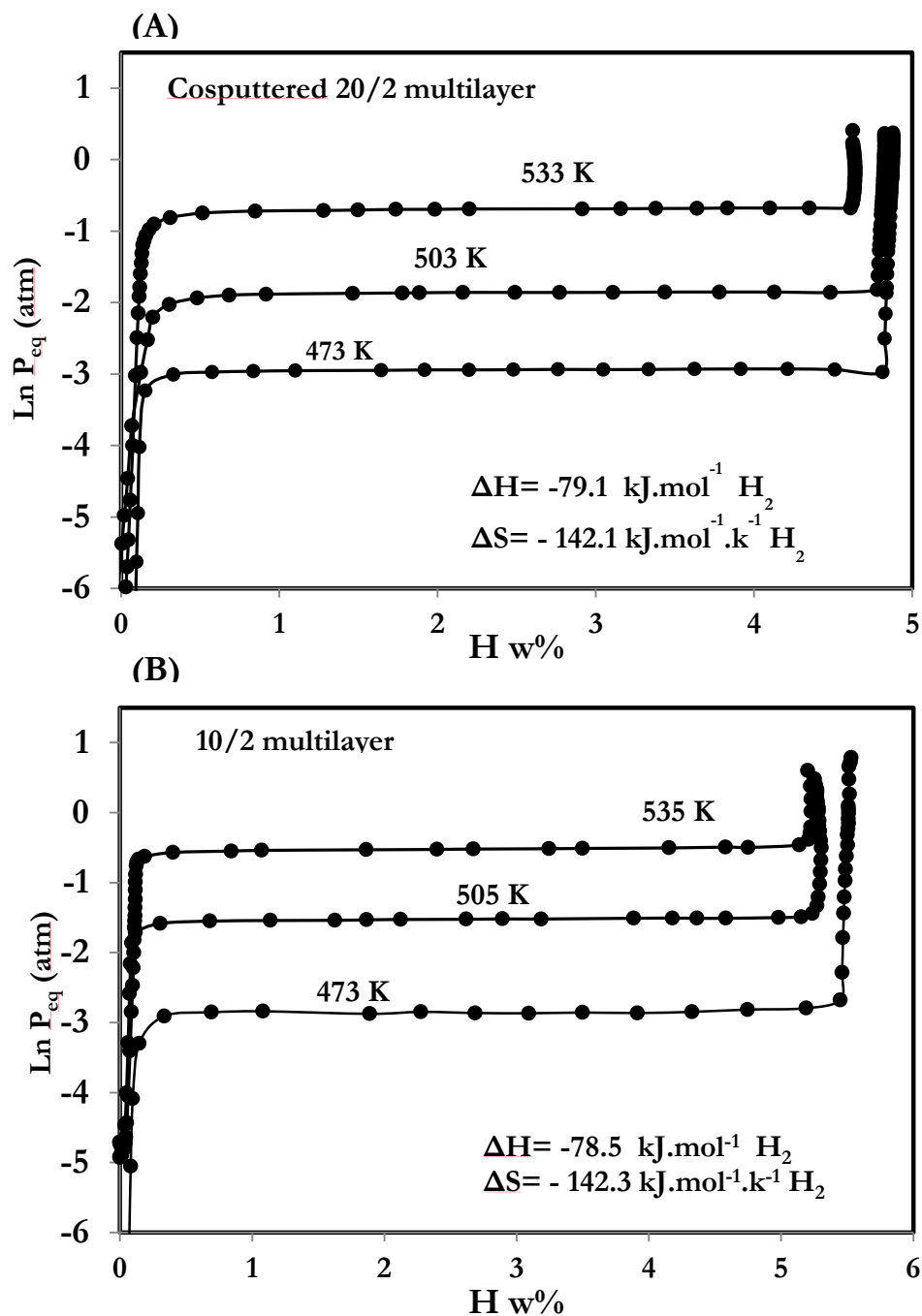


Figure 2-4 Pressure-composition isotherms of (A) cosputtered 20/2 and (B) 10/2 multilayers.

In the current system we evaluated the possible thermodynamics alteration by performing a PCT measurement. Figure 2-4 shows desorption pressure-composition isotherms at three different temperatures for the 10/2 and the 20/2 multi-layer

samples and after 20 activation cycles at 473 K. For the 10/2, the plateau pressures are 0.05, 0.20 and 0.44 bar at 473, 505 and 535 K, respectively, giving a value for the heat of hydride formation of -78.5 kJ/H₂ molecule. For the 20/2, the plateau pressures are 0.05, 0.14 and 0.41 bar at 473, 503 and 533 K, respectively, giving a value for the heat of hydride formation of -79.1 kJ/H₂ molecule. These values are in good agreement with values for the hydrogenation enthalpy of Mg reported widely in the literature [41] and no sign of destabilization is observed. Thus, the improved performance of these samples is merely kinetics and the thermodynamics is not altered.

2.3.3 Microstructural analysis

Bright Field and dark field TEM images of a 10/2 multilayer sample after 10 sorption cycles are depicted in figure 2-5 along with its selected area diffraction pattern (SAD) and a high resolution image showing a stack of a few Mg and AlTi layers. The diffraction pattern represents [121] zone axis of hcp magnesium. The high resolution image shows how Mg and AlTi layers are in intimate contact with a smooth transition in the interface. After 10 cycles, as can be seen in figure 2-5A some deformation is apparent in some parts of the sample. Considering the nominal layers thickness, a small expansion is observed. Figure 2-5E show a cross section SEM images of 10/2 sample demonstrating a solid structure of multilayer.

In the as deposited state, as shown in figure 2-6B, (002) peak of Mg from 20/2 multilayer is close to that of hexagonal Mg, while for the co-sputtered 20/2 this peak is shifted to 35° indicating complete solid solution of Ti and Al with Mg. This shift

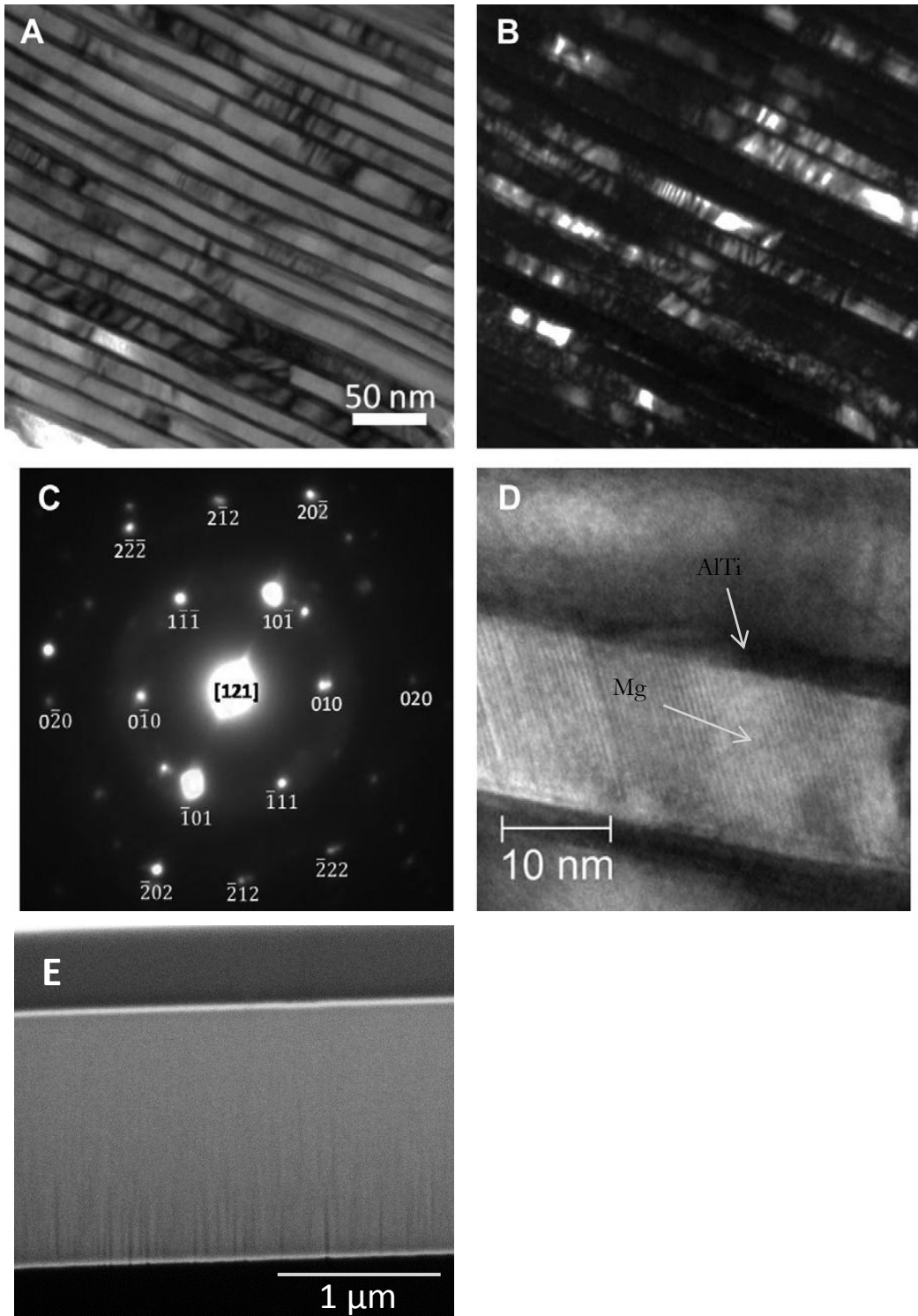


Figure 2-5 (A) Bright field and (B) dark field images and (C) corresponding SAD of 10/2 multilayer after 10 cycles. The SAD shows a [121] zone axis of Mg and the bright field is taken using (010) reflection. (D) HRTEM image shows intimate contact between Mg atomic planes and AlTi amorphous/nanocrystalline layers. (E) Cross section SEM image of as-prepared 10/2 multilayer.

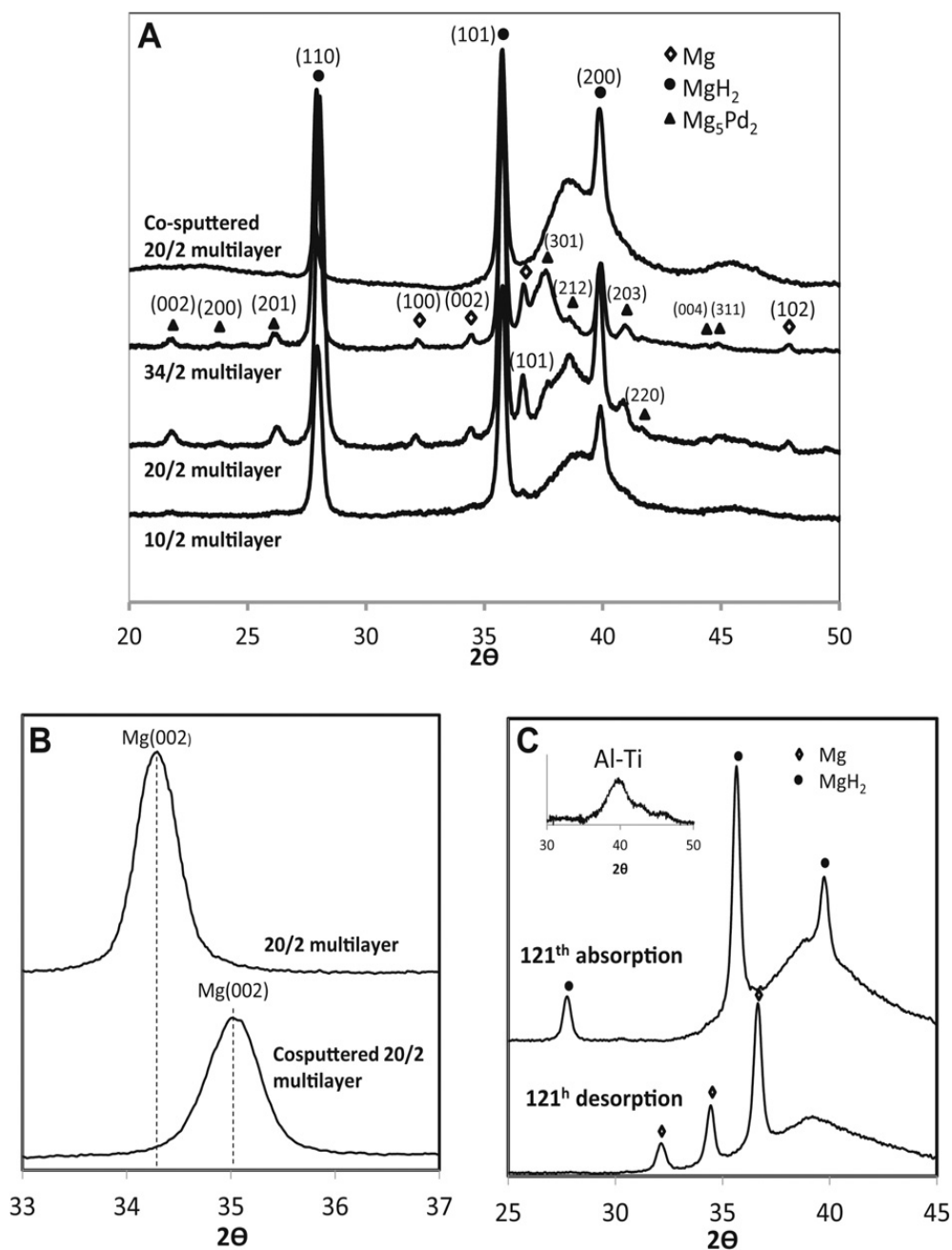


Figure 2-6 (A) X-ray diffraction patterns of the studied multilayer composites after cycling; (B) a comparison between as deposited samples 20/2 and co-sputtered 20/2 showing the shift in Mg(002) crystalline peak from 34.3 to 35 due to formation of metastable solid solution between Mg, Al and Ti through sputtering; (C) XRD pattern of a multilayer sample with extra thick (50 nm) Al-Ti layer after 121 sorption cycles before and after cycling to highlight the AlTi intermetallic nanocrystalline/amorphous hump. The inset in (C) shows XRD scan of a 50 nm co-sputtered Al-Ti film treated at same condition as the multilayers in absorbed state.

in the position of (002) peak is in agreement with Vegard's law. Segregation of alloying element at elevated temperatures and in the presence of hydrogen has been reported elsewhere [42]. After cycling, as seen in figure 2-6A, all assigned MgH_2 reflections in samples with pure Mg layers represent rutile $\alpha\text{-MgH}_2$. Since no shift in the position of hydride peaks is observed in the co-sputtered case, we can conclude that neither Al nor Ti are in solid solution with Mg and they most probably have formed intermetallic AlTi. Formation of AlTi intermetallic is reported in a similar condition for co-sputtered Mg-Al15Ti15 thin film [36]. Despite the attempt to prohibit the interaction of Mg and Pd using Ta, Mg_3Pd_2 reflections with the strongest peaks of (301), (212), and (201), also appear in the diffraction patterns of 20/2 and 34/2 multilayers. However, the patterns of 10/2 and co-sputtered 20/2 multilayers do not show evidence of Mg-Pd compound formation. The presence of Mg in the fully absorbed state of 20/2, and 34/2 is because there is still some unreacted Mg left when the 0.005 wt. %/min cut off rate is reached, due to slower sorption kinetics in these composites. Note that the samples were tested right after kinetic measurements.

The hump appeared in the X-ray diffraction pattern of samples is most likely related to an amorphous or nanocrystalline AlTi phase. However, it overlaps with Mg_3Pd_2 reflections. To have a more intense peak of AlTi, a 10/2 sample with an extra thick AlTi layer (50 nm) below Pd/Ta protective layer was produced and cycled under the same conditions. The 121st ab-and desorption are shown in Fig. 2-6C. In the absence of Mg_3Pd_2 , aside from MgH_2 and Mg, the only detectable phase which has a broad

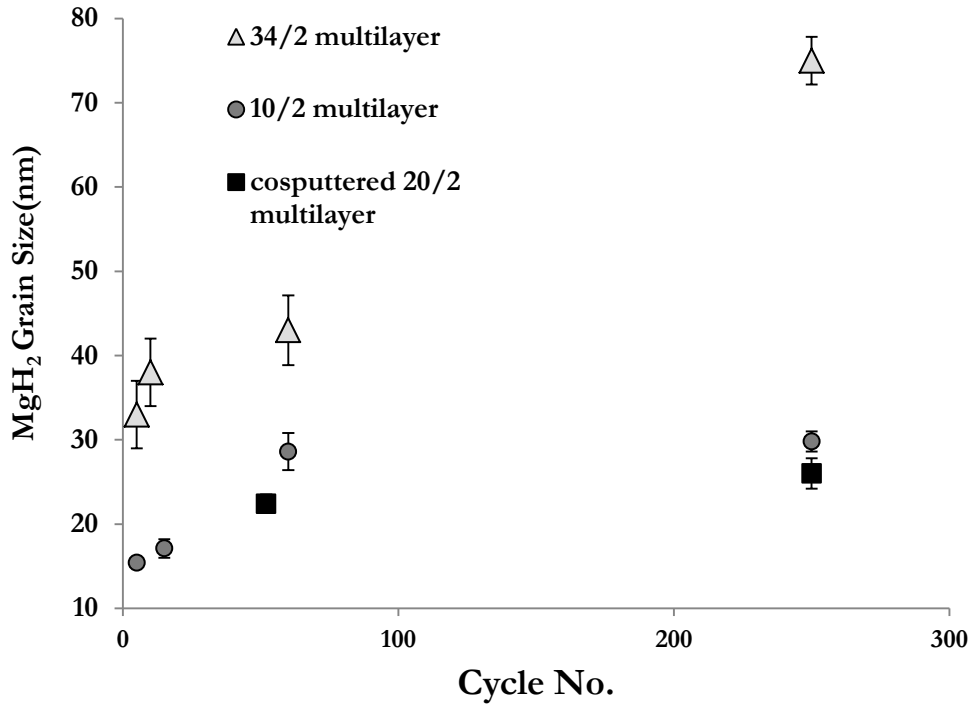


Figure 2-7 Variation of MgH₂ grain size as a function of cycle number.

reflection centered at $2\Theta = 39^\circ$ is suggested to be amorphous/nanocrystalline AlTi intermetallic compound. Also, a 50 nm thick film of co-sputtered Al-Ti was produced and treated with the same condition as absorbed samples and a similar hump was observed as shown in the inset of Fig 2-6C, emphasizing formation of an amorphous/nanocrystalline AlTi phase.

The variation of MgH₂ grain size as a function of cycle number is depicted in figure 2-7. For 34/2 multilayer, the grain size increases from 32 to 75 nm during cycling. However, the grain growth is much slower for 10/2 where thin Mg layers are constrained by AlTi layers; which shows a growth from 15 to about 30 nm during activation and remains almost constant through the rest of the cycles. Grain growth is less pronounced for co-sputtered 20/2 multilayer and only reaches 25 nm by the

end of cycling. It is also worth mentioning that the XRD results from this sample at the early stages of cycling demonstrated the textured characteristics of sputtered thin films and the grain size measurements were not conclusive.

Upon cycling, the initial structure of multilayers with continuous Mg and AlTi layers transforms to a porous structure. It has been shown that upon hydrogenation of a Mg layer capped with Pd at 373 K and 0.2 MPa H₂, the Mg film swells and after dehydrogenation (at 343-423 K), the Mg film retains the swelled thickness by incorporating voids [43]. A similar phenomenon was seen in present multilayer composites as seen in cross sectional SEM images of samples. The SEM micrograph of 10/2, 20/2, co-sputtered 20/2 and 34/2 samples after 250 cycles are illustrated in figures 2-8 and 2-9. Macroscopic views of 10/2, co-sputtered 20/2 and to some extent 20/2 multilayers in figure 2-8A, C and figure 2-9A, show that these multilayer samples could keep the initial thin film forms with almost no disintegration. As for 34/2 sample, the original films are disintegrated into small flakes and the top Ta/Pd layers are completely removed as seen in images 2-9D.

The cross section images of 10/2, co-sputtered 20/2 multi-layers after 250 cycles (figure 2-8B and D respectively) show that despite the fact that repetitive volume expansion/ contraction during sorption cycling causes the AlTi barrier layers to severely deform, the layered structure is somehow preserved and the sintering occurs in very localized sections of some neighboring layers. Even the Ta/Pd layers are seen intact which is in agreement with absence of Mg-Pd compound in the XRD results. However, for 20/2 multilayer (figure 2-9B) with the same configuration as co-

sputtered 20/2, isolated Mg particles has formed. Comparing the structure of co-sputtered 20/2 and 20/2 samples suggests the significant effect of Al and Ti addition to Mg layers of co-sputtered 20/2 on the integrity of multilayers. It should be noted that microstructure becomes porous after cycling compared with as deposited structure (Figure 2-5E)

STEM Bright-field and high annular dark field images of co-sputtered 20/2 sample after 60 cycles along with the elemental mapping of Mg, Ti and Al are shown in figure 2-10. Note that in order to prepare electron transparent particles for TEM, original films had to be pulverized by mechanical means. These images show that even after mechanical pulverization particles preserved their layered structure. Z-contrast high annular dark field STEM images show brighter spots where Al and/or Ti are present in Mg matrix. This is further confirmed by EDS elemental maps given in figure 2-10. Figure 2-11 shows a large Mg particle after 260 cycles of co-sputtered 20/2. Higher concentration of Al and Ti on the edges of the particle as shown in elemental map of Al and Ti in figure 2-11, suggests formation of nanometric AlTi particles on the surface; since according to XRD results and thermodynamics data, they do not stay in solid solution with Mg when conditions for equilibrium reached at cycling temperature.

2.4 Discussion

Constraining the Mg layer by reducing its thickness and employing more AlTi layers resulted in better performance as seen for multilayers of 10 nm Mg thickness (10/2)

as opposed to 20/2 and 34/2. Adding Al and Ti to Mg layers enabled co-sputtered 20/2 composite to have a comparable performance, if not improved, with 10/2 without sacrificing much capacity. Note that co-sputtered 20/2 and 10/2 have relatively the same amount of Al-Ti catalyst addition. Using AlTi layers proved effective in keeping the multilayer Mg-based thin films from disintegration during cycling. However, although successful size limitation of Mg grains to below 50 nm, no appreciable thermodynamic destabilization occurred. The kinetic data shown in figure 2-1 and 2-3 when combined with characterization data shown in figure 2-7

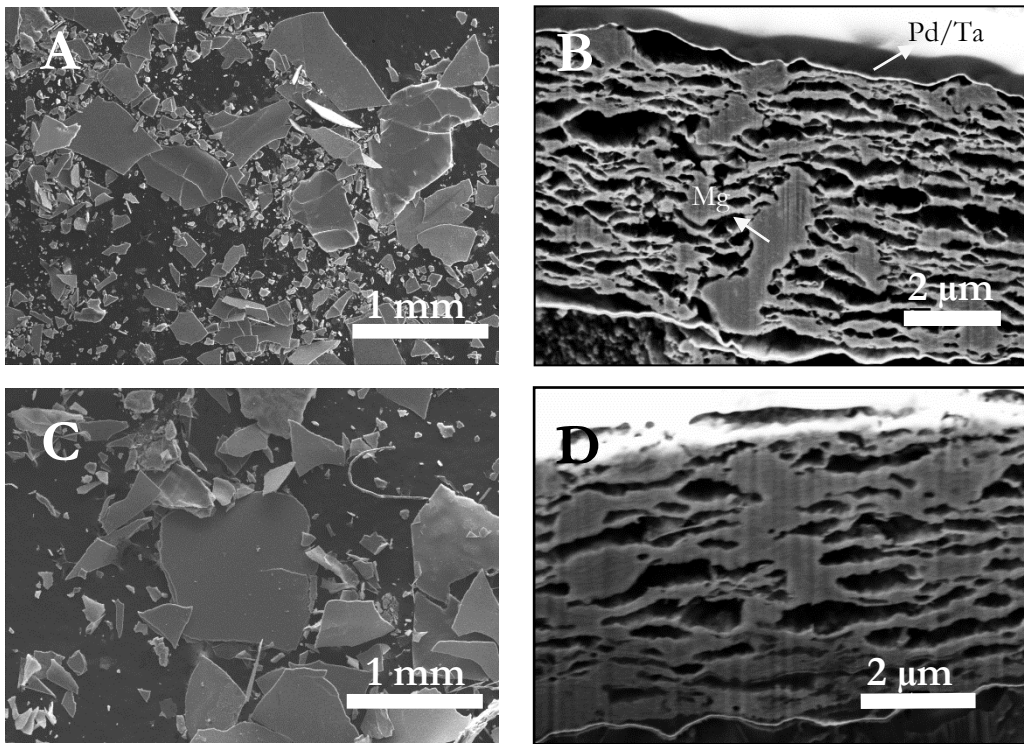


Figure 2-8 SEM images of cycled composites: (A) macroscopic view of 10/2 showing multilayer films preserving their original shapes, (B) FIB image of the cross section showing expansion and void formation between the AlTi layers and a few particles diffused through the AlTi layers and coalesced; (C) macroscopic view of co-sputtered 20/2 showing multilayer films preserving their original shapes, (D) FIB image of the cross sectional view of co-sputtered 20/2 showing void formation between the AlTi layers.

and 2-8 suggest that the co-sputtered 20/2 sample with the most stable kinetics was also the most resistant against decrepitation. The AlTi layers in this sample kept the Mg particles from expansion in thickness direction to some extent, as can be seen in figure 2-8D, while AlTi particles formed on the surface and probably in grain boundaries (figure 2-10 and 2-11) kept the grains from growing too large and coalescing together.

Cross sectional image shown in figure 2-8B and D and figure 2-9B suggest that formation of small voids is a necessary process for activation. It also suggests that for multilayers with higher number of layers (e.g. 10/2) the reason the activation takes higher number of cycles, as implied by figure 2-3, lies in the difficulty of void formation in more compact samples of thinner Mg layers. It seems that further cycling induces a network of voids which facilitate hydrogen transportation. Thus, we attribute the activation period to the cycles required for the material to reach a steady state cyclability in which the hydrogen transportation through voids is easily achieved and more AlTi surfaces are exposed to hydrogen. This process leads to faster sorption rates after activation. It should be noted that formation of voids is a result of expansion of Mg layers during hydrogenation and their contraction in the reverse reaction.

It can be seen in the SEM images of 10/2 (figure 2-8B) and 20/2 (figure 2-9B) that magnesium layers can coalesce and form relatively large Mg particles and lose their contact with AlTi catalyst layers. This effect is more severe for 20/2 multilayer which has more isolated Mg particles. Thicker Mg layers can induce higher expansion

stresses. In this scenario the dissociated hydrogen has to diffuse through larger Mg particles, which in turn have larger grains. In larger grains hydrogen diffusion could be a sluggish process due to low diffusivity of hydrogen through the growing hydride layer [44, 45]. However, samples 20/2 and co-sputtered 20/2 with identical structures and number of layers behaved differently in activation. From the inset in figure 2-3A it is clear that the former needs approximately 25 cycles to activate while it takes about 15 cycles for the latter to fully activate.

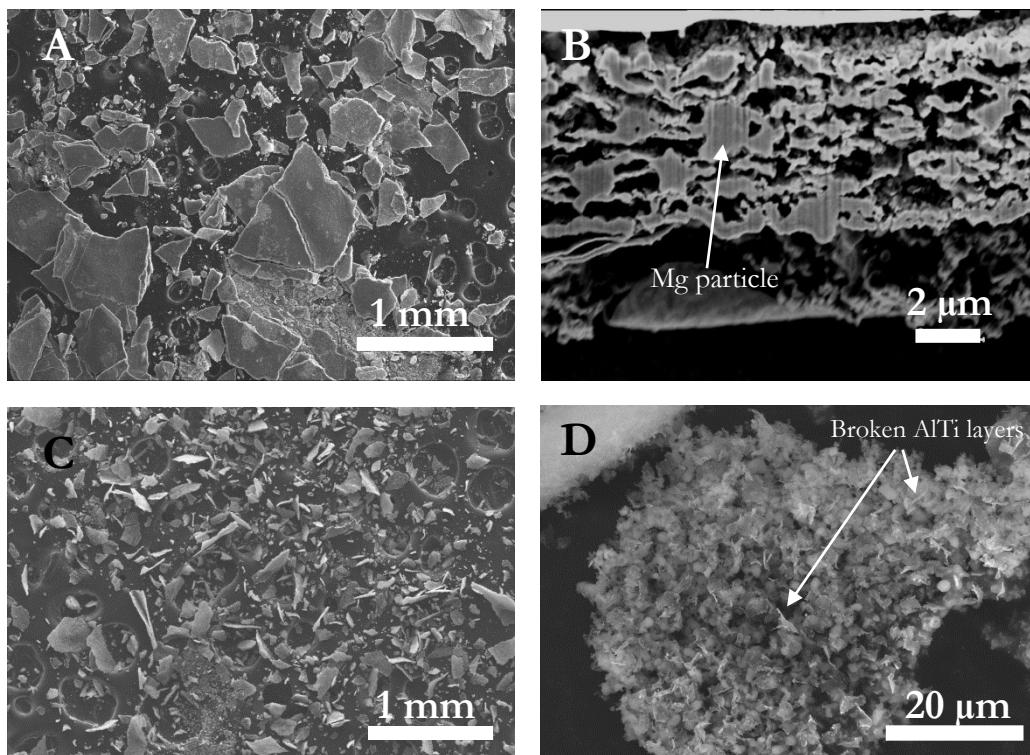


Figure 2-9 (A) macroscopic view of 20/2 multilayer showing some disintegration in original films shapes, (B) FIB image of the cross section view of 20/2 showing severe expansion and void formation between the AlTi layers and deformation and rupture of AlTi layers while new large interlayer particles formed; (C) macroscopic view of 34/2 showing original films disintegrated into small flakes, (D) microscopic top view of the 34/2 flakes showing spongy structure after cycling.

On the other hand, the time to reach 90 wt.% capacity plot shows that after a stable

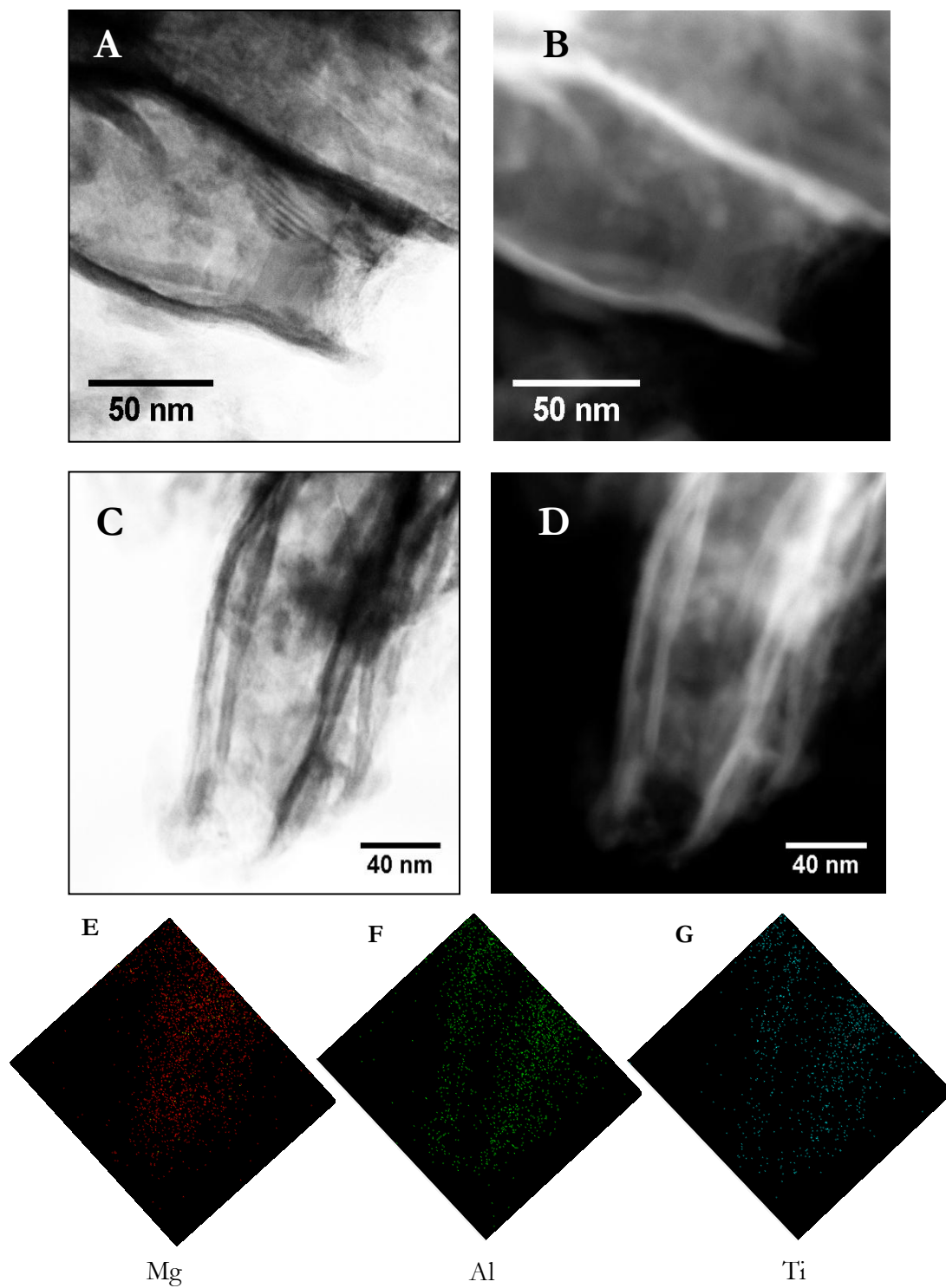


Figure 2-10 (A,C) Bright-field and (B,D)high angle annular dark field images of co-sputtered 20/2 sample after 60 cycles along with the elemental mapping of Mg, Ti and Al (E,F,G).

cycling period, the 10/2, 20/2 and 34/2 samples starts to degrade slightly and sorption increases consequently. Besides, IBA grain analysis results show that in degraded samples, grain growth is a common phenomenon. 10/2 has better performance than 34/2 multi-layer by further constraining Mg layers and restraining grain growth. As seen in figure 2-7, the grain size for co-sputtered 20/2 multilayer does not change in an appreciable manner from cycle 60 to 250 and as figure 2-3 implies, the corresponding sorption times remain steady during cycling. This indicates that the cycling stability of the material is to some extent dependent on its resistant against grain growth which in general is a bi-product of structural disintegration.

Similar to what suggested for the role of CrV precipitates in Mg-Cr-V co-sputtered thin films [46], AlTi particles formed in co-sputtered 20/2 composites can have a positive effect on Mg(H₂) grain size in a way that a network structure of AlTi in grain boundaries reduces MgH₂ grain size and limits the formation of blocking hydride layer. A similar behavior has also been observed in studying multilayers of Mg/FeTi [27]. When compared to cosputtered Mg-Fe-Ti thin films, FeTi layers seemed not to be as effective as FeTi particles to restrict the grain growth. Similar to the present case, magnesium grains grew more rapidly in Mg/FeTi multilayer than in Mg-Fe-Ti co-sputtered thin films. It seems that FeTi particles formed in grain boundaries were responsible for limiting the Mg grain growth. Here, similarly, AlTi nano-particles were detected using STEM combined with HAADF and EDS and are shown in figure 2-10. The SEM image of co-sputtered 20/2 also shows that

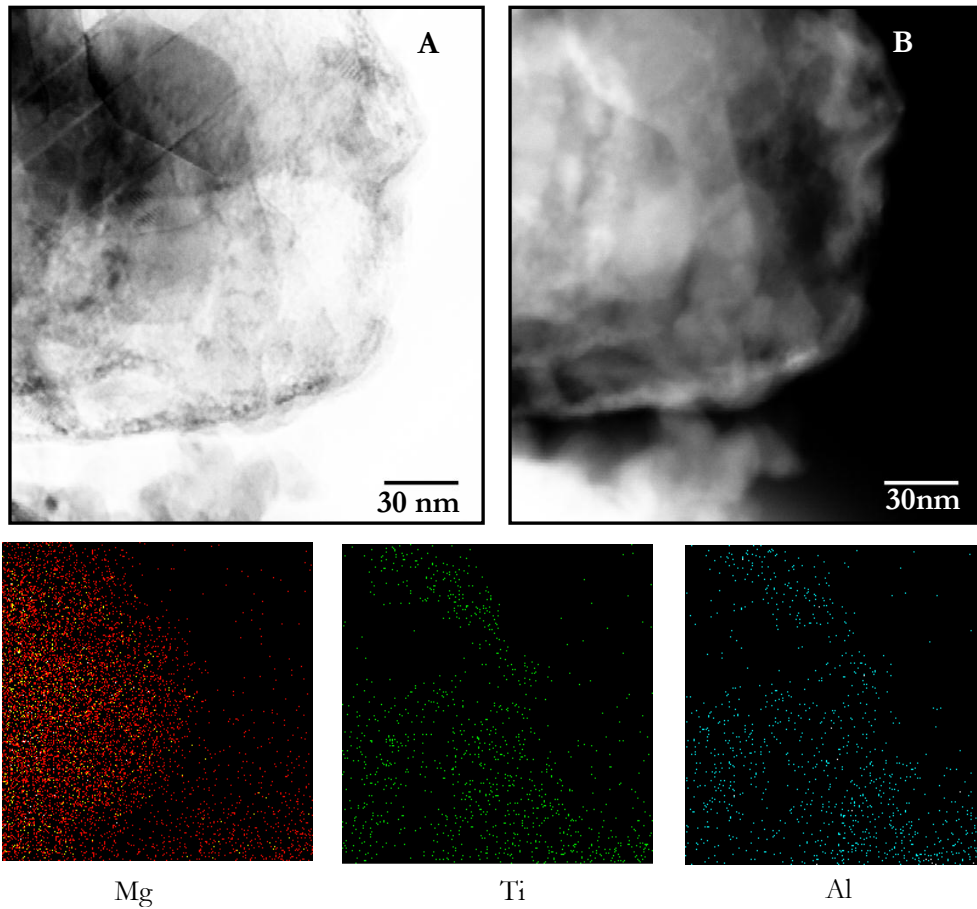


Figure 2-11 (A) STEM Bright-field and (B) high angle annular dark field images of a Mg particle of co-sputtered 20/2 sample after 260 cycles along with the elemental mapping of Mg, Ti and Al.

agglomeration of magnesium is prevented when compared to 10/2 and 20/2 multilayers.

When Al and Ti are added to the layers of magnesium, the network structure of precipitated AlTi nano-particles would act as a barrier to boundary motion and limit the formation of large isolated pure Mg particles which are detrimental to performance of the material. This exceptional behavior of AlTi can be well understood when it is known that diffusion of hydrogen in AlTi is much faster than

Mg [37] helping rapid hydrogenation of Mg through the network of AlTi nanoparticles and also AlTi layers. More interestingly, the 2 nm AlTi will not be affected by hydrogen since it has negligible affinity for hydrogen and can remain intact during cycling, sustaining its catalytic activity and mechanical integrity.

By combining these effects we could produce multilayers with controlled expansion of Mg layers by constraining them with AlTi layers and controlled grain size by incorporating nanometric AlTi particles on the surface of Mg grains and in grain boundaries. The sputtered multilayer composites have identical cycling performance compared to the single layer co-sputtered thin films, and the resistance of multilayer structure to disintegration protect them against agglomeration and sintering which leads to degradation in storage systems.

2.5 Summary

The multilayers of Mg-AlTi showed cyclability with remarkable kinetics. By restricting the particle size and controlling the grain size of Mg in multilayers of cosputtered Mg-Al-Ti sandwiched by AlTi layers we were able to achieve composites with high cycling stability as well as mechanical integrity. We showed that Al and Ti, when cosputtered, form an amorphous/nanocrystalline AlTi intermetallic that does not react with magnesium and is mechanically stable enough to preserve multilayers during hydrogen sorption cycling. In the case of pure Mg layers, when the thickness of layers is higher than 20 nm, although activation occurs faster, the degradation is also more severe. For multilayers of 34 nm Mg, expansion of Mg layers upon cycling

leads in disintegration of multilayers and formation of porous flakes. By combining the effect of AlTi layers in constraining the Mg layers from uncontrolled expansion and the effect of AlTi particles in limiting Mg grain growth we were able to produce composites with rapid sorption kinetics and high cyclability and mechanical stability in over 250 cycles.

2.6 References

- [1] X. Tan, M. Danaie, W. P. Kalisvaart, and D. Mitlin, "The influence of Cu substitution on the hydrogen sorption properties of magnesium rich Mg-Ni films," *International Journal of Hydrogen Energy*, vol. 36, no. 3, pp. 2154–2164, Feb. 2011.
- [2] M. Tanniru, D. K. Slattery, and F. Ebrahimi, "A study of stability of MgH₂ in Mg–8at%Al alloy powder," *International Journal of Hydrogen Energy*, vol. 35, no. 8, pp. 3555–3564, Apr. 2010.
- [3] J. P. Lei, H. Huang, X. L. Dong, J. P. Sun, B. Lu, M. K. Lei, Q. Wang, C. Dong, and G. Z. Cao, "Formation and hydrogen storage properties of in situ prepared Mg–Cu alloy nanoparticles by arc discharge," *International Journal of Hydrogen Energy*, vol. 34, no. 19, pp. 8127–8134, Oct. 2009.
- [4] J. J. Vajo, F. Mertens, C. C. Ahn, Bowman, and B. Fultz, "Altering Hydrogen Storage Properties by Hydride Destabilization through Alloy Formation: LiH and MgH₂ Destabilized with Si," *J. Phys. Chem. B*, vol. 108, no. 37, pp. 13977–13983, 2004.
- [5] J. J. Reilly and R. H. Wiswall, "Reaction of hydrogen with alloys of magnesium and nickel and the formation of Mg₂NiH₄," *Inorg. Chem.*, vol. 7, no. 11, pp. 2254–2256, 1968.
- [6] J. J. Reilly and R. H. Wiswall, "Reaction of hydrogen with alloys of magnesium and copper," *Inorg. Chem.*, vol. 6, no. 12, pp. 2220–2223, 1967.

- [7] B. Yang, Y. He, and Y. Zhao, "Concentration-dependent hydrogen diffusion in hydrogenation and dehydrogenation of vanadium-coated magnesium nanoblades," *International Journal of Hydrogen Energy*, vol. 36, no. 24, pp. 15642–15651, Dec. 2011.
- [8] S. Barcelo and S. S. Mao, "High throughput optical characterization of alloy hydrogenation," *International Journal of Hydrogen Energy*, vol. 35, no. 13, pp. 7228–7231, Jul. 2010.
- [9] M. Pozzo and D. Alfè, "Hydrogen dissociation and diffusion on transition metal (= Ti, Zr, V, Fe, Ru, Co, Rh, Ni, Pd, Cu, Ag)-doped Mg(0001) surfaces," *International Journal of Hydrogen Energy*, vol. 34, no. 4, pp. 1922–1930, Feb. 2009.
- [10] N. Hanada, T. Ichikawa, and H. Fujii, "Catalytic Effect of Nanoparticle 3d-Transition Metals on Hydrogen Storage Properties in Magnesium Hydride MgH₂ Prepared by Mechanical Milling," *J. Phys. Chem. B*, vol. 109, no. 15, pp. 7188–7194, 2005.
- [11] G. Liang, J. Huot, S. Boily, A. Van Neste, and R. Schulz, "Catalytic effect of transition metals on hydrogen sorption in nanocrystalline ball milled MgH₂-Tm (Tm=Ti, V, Mn, Fe and Ni) systems," *Journal of Alloys and Compounds*, vol. 292, no. 1–2, pp. 247–252, Nov. 1999.
- [12] R. L. Holtz and M. A. Imam, "Hydrogen storage characteristics of ball-milled magnesium-nickel and magnesium-iron alloys," *Journal of Materials Science*, vol. 34, no. 11, pp. 2655–2663, 1999.
- [13] S. Kwon, S. Baek, D. R. Mumm, S.-H. Hong, and M. Song, "Enhancement of the hydrogen storage characteristics of Mg by reactive mechanical grinding with Ni, Fe and Ti," *International Journal of Hydrogen Energy*, vol. 33, no. 17, pp. 4586–4592, Sep. 2008.
- [14] B. S. Amirkhiz, M. Danaie, M. Barnes, B. Simard, and D. Mitlin, "Hydrogen Sorption Cycling Kinetic Stability and Microstructure of Single-Walled Carbon Nanotube (SWCNT) Magnesium Hydride (MgH₂) Nanocomposites," *J. Phys. Chem. C*, vol. 114, no. 7, pp. 3265–3275, 2010.
- [15] B. S. Amirkhiz, M. Danaie, and D. Mitlin, "The influence of SWCNT-metallic nanoparticle mixtures on the desorption properties of milled MgH₂ powders," *Nanotechnology*, vol. 20, no. 20, p. 204016, May 2009.

- [16] S. Aminorroaya, H. K. Liu, Y. Cho, and A. Dahle, "Microstructure and activation characteristics of Mg–Ni alloy modified by multi-walled carbon nanotubes," *International Journal of Hydrogen Energy*, vol. 35, no. 9, pp. 4144–4153, May 2010.
- [17] H. Fritzsche, W. P. Kalisvaart, B. Zahiri, R. Flacau, and D. Mitlin, "The catalytic effect of Fe and Cr on hydrogen and deuterium absorption in Mg thin films," *International Journal of Hydrogen Energy*, vol. 37, no. 4, pp. 3540–3547, Feb. 2012.
- [18] B. S. Amirkhiz, B. Zahiri, P. Kalisvaart, and D. Mitlin, "Synergy of elemental Fe and Ti promoting low temperature hydrogen sorption cycling of magnesium," *International Journal of Hydrogen Energy*, vol. 36, no. 11, pp. 6711–6722, Jun. 2011.
- [19] B. Zahiri, B. S. Amirkhiz, and D. Mitlin, "Hydrogen storage cycling of MgH₂ thin film nanocomposites catalyzed by bimetallic Cr–Ti," *Applied Physics Letters*, vol. 97, no. 8, pp. 083106–083106–3, Aug. 2010.
- [20] B. Zahiri, B. S. Amirkhiz, M. Danaie, and D. Mitlin, "Bimetallic Fe–V catalyzed magnesium films exhibiting rapid and cycleable hydrogenation at 200 °C," *Applied Physics Letters*, vol. 96, no. 1, pp. 013108–013108–3, Jan. 2010.
- [21] B. Zahiri, C. T. Harrower, B. Shalchi Amirkhiz, and D. Mitlin, "Rapid and reversible hydrogen sorption in Mg–Fe–Ti thin films," *Applied Physics Letters*, vol. 95, no. 10, pp. 103114–103114–3, Sep. 2009.
- [22] M. Danaie, C. Mauer, D. Mitlin, and J. Huot, "Hydrogen storage in bulk Mg–Ti and Mg–stainless steel multilayer composites synthesized via accumulative roll-bonding (ARB)," *International Journal of Hydrogen Energy*, vol. 36, no. 4, pp. 3022–3036, Feb. 2011.
- [23] J. Dufour and J. Huot, "Rapid activation, enhanced hydrogen sorption kinetics and air resistance in laminated Mg–Pd 2.5 at.%, " *Journal of Alloys and Compounds*, vol. 439, no. 1–2, pp. L5–L7, Jul. 2007.
- [24] J. Dufour and J. Huot, "Study of Mg₆Pd alloy synthesized by cold rolling," *Journal of Alloys and Compounds*, vol. 446–447, no. 0, pp. 147–151, Oct. 2007.
- [25] S. Pedneault, J. Huot, and L. Roué, "Nanostructured Mg₂Ni materials prepared by cold rolling and used as negative electrode for Ni–MH batteries," *Journal of Power Sources*, vol. 185, no. 1, pp. 566–569, Oct. 2008.

- [26] S. Couillaud, H. Enoki, S. Amira, J. L. Bobet, E. Akiba, and J. Huot, "Effect of ball milling and cold rolling on hydrogen storage properties of nanocrystalline TiV_{1.6}Mn_{0.4} alloy," *Journal of Alloys and Compounds*, vol. 484, no. 1–2, pp. 154–158, Sep. 2009.
- [27] W. P. Kalisvaart, A. Kubis, M. Danaie, B. S. Amirkhiz, and D. Mitlin, "Microstructural evolution during hydrogen sorption cycling of Mg–FeTi nanolayered composites," *Acta Materialia*, vol. 59, no. 5, pp. 2083–2095, Mar. 2011.
- [28] S. Y. Ye, S. L. I. Chan, L. Z. Ouyang, and M. Zhu, "Hydrogen storage and structure variation in Mg/Pd multi-layer film," *Journal of Alloys and Compounds*, vol. 504, no. 2, pp. 493–497, Aug. 2010.
- [29] S. Barcelo, M. Rogers, C. P. Grigoropoulos, and S. S. Mao, "Hydrogen storage property of sandwiched magnesium hydride nanoparticle thin film," *International Journal of Hydrogen Energy*, vol. 35, no. 13, pp. 7232–7235, Jul. 2010.
- [30] P. Jain, A. Jain, D. Vyas, R. Verma, S. A. Khan, and I. P. Jain, "The effects of Ni and Mg₂Ni interlayer on hydrogenation properties of Pd sandwiched Mg films," *Journal of Alloys and Compounds*, vol. 509, no. 5, pp. 2105–2110, Feb. 2011.
- [31] T. K. Nielsen, F. Besenbacher, and T. R. Jensen, "Nanoconfined hydrides for energy storage," *Nanoscale*, vol. 3, no. 5, p. 2086, 2011.
- [32] S. X. Tao, P. H. L. Notten, R. A. van Santen, and A. P. J. Jansen, "First-principles predictions of potential hydrogen storage materials: Nanosized Ti(core)/Mg(shell) hydrides," *Phys. Rev. B*, vol. 83, no. 19, p. 195403, May 2011.
- [33] S. X. Tao, P. H. L. Notten, R. A. van Santen, and A. P. J. Jansen, "Fluorite transition metal hydride induced destabilization of the MgH₂ system in MgH₂/TMH₂ multilayers (TM=Sc, Ti, V, Cr, Y, Zr, Nb, La, Hf)," *Phys. Rev. B*, vol. 82, no. 12, p. 125448, 2010.
- [34] A. Baldi, V. Palmisano, M. Gonzalez-Silveira, Y. Pivak, M. Slaman, H. Schreuders, B. Dam, and R. Griessen, "Quasifree Mg–H thin films," *Applied Physics Letters*, vol. 95, no. 7, pp. 071903–071903–3, Aug. 2009.
- [35] A. Baldi, M. Gonzalez-Silveira, V. Palmisano, B. Dam, and R. Griessen, "Destabilization of the Mg-H System through Elastic Constraints," *Phys. Rev. Lett.*, vol. 102, no. 22, p. 226102, Jun. 2009.
- [36] W. P. Kalisvaart, C. T. Harrower, J. Haagsma, B. Zahiri, E. J. Lubber, C. Ophus, E. Poirier, H. Fritzsche, and D. Mitlin, "Hydrogen storage in binary and

ternary Mg-based alloys: A comprehensive experimental study,” *International Journal of Hydrogen Energy*, vol. 35, no. 5, pp. 2091–2103, Mar. 2010.

[37] S. Hao, “The TiAl channel mechanism for enhanced (de)hydrogenation kinetics in Mg-based films,” *Applied Physics Letters*, vol. 97, no. 11, pp. 111905–111905–3, Sep. 2010.

[38] X. Tan, C. T. Harrower, B. S. Amirkhiz, and D. Mitlin, “Nano-scale bi-layer Pd/Ta, Pd/Nb, Pd/Ti and Pd/Fe catalysts for hydrogen sorption in magnesium thin films,” *International Journal of Hydrogen Energy*, vol. 34, no. 18, pp. 7741–7748, Sep. 2009.

[39] R. W. P. Wagemans, J. H. van Lenthe, P. E. de Jongh, A. J. van Dillen, and K. P. de Jong, “Hydrogen Storage in Magnesium Clusters: Quantum Chemical Study,” *J. Am. Chem. Soc.*, vol. 127, no. 47, pp. 16675–16680, 2005.

[40] A. Baldi, G. K. Pálsson, M. Gonzalez-Silveira, H. Schreuders, M. Slaman, J. H. Rector, G. Krishnan, B. J. Kooi, G. S. Walker, M. W. Fay, B. Hjörvarsson, R. J. Wijngaarden, B. Dam, and R. Griessen, “Mg/Ti multilayers: Structural and hydrogen absorption properties,” *Phys. Rev. B*, vol. 81, no. 22, p. 224203, Jun. 2010.

[41] R. Griessen and T. Riesterer, “Heat of formation models,” in *Hydrogen in Intermetallic Compounds I*, vol. 63, L. Schlapbach, Ed. Springer Berlin / Heidelberg, 1988, pp. 219–284.

[42] N. Bazzanella, R. Checchetto, and A. Miotello, “Catalytic effect of mixed Zr–Fe additives on the hydrogen desorption kinetics of MgH₂,” *Applied Physics Letters*, vol. 92, no. 5, pp. 051910–051910–3, Feb. 2008.

[43] J. A. Dura, S. T. Kelly, P. A. Kienzle, J.-H. Her, T. J. Udovic, C. F. Majkrzak, C.-J. Chung, and B. M. Clemens, “Porous Mg formation upon dehydrogenation of MgH₂ thin films,” *Journal of Applied Physics*, vol. 109, no. 9, pp. 093501–093501–7, May 2011.

[44] M. S. Conradi, M. P. Mendenhall, T. M. Ivancic, E. A. Carl, C. D. Browning, P. H. L. Notten, W. P. Kalisvaart, P. C. M. M. Magusin, R. C. Bowman Jr., S.-J. Hwang, and N. L. Adolphi, “NMR to determine rates of motion and structures in metal-hydrides,” *Journal of Alloys and Compounds*, vol. 446–447, no. 0, pp. 499–503, Oct. 2007.

[45] D. S. Sholl, "Using density functional theory to study hydrogen diffusion in metals: A brief overview," *Journal of Alloys and Compounds*, vol. 446–447, no. 0, pp. 462–468, Oct. 2007.

[46] P. Kalisvaart, E. Lubber, H. Fritzsche, and D. Mitlin, "Effect of alloying magnesium with chromium and vanadium on hydrogenation kinetics studied with neutron reflectometry," *Chemical Communications*, vol. 47, no. 14, p. 4294, 2011.

3 Thermodynamics destabilization of Mg-based multilayers for hydrogen storage

3.1 Introduction

As described in chapter 1, one of the main barriers for magnesium as material for hydrogen storage is its high affinity with hydrogen, which results in formation of strong M-H bond. Thus, high temperatures are required to release the absorbed hydrogen from hydride. For magnesium with formation enthalpy of -76 kJ/mol H_2 , the hydrogen desorption pressure of 1 bar can be obtained at $250 \text{ }^\circ\text{C}$.

To tune the thermodynamics properties of magnesium and lower the (de)hydrogenating reaction, one may use chemical methods to alloy magnesium [1, 2]. The additives can form alloys or compounds with Mg in either the hydrogenated or dehydrogenated state. Mg_2Ni , as a well-known example, is transformed to Mg_2NiH_4 upon hydrogenation with the reversible capacity of 3.6 wt% hydrogen and 1 bar plateau pressure at $245 \text{ }^\circ\text{C}$ [3]. Another example is Mg-Al alloy which transforms to Al and MgH_2 upon hydrogenation. The plateau pressure for this system is three times higher than that of pure Mg at $280 \text{ }^\circ\text{C}$ [4]. Similar to Mg-Al system, studies on Mg-Si have shown a considerable destabilization of the hydride. The dehydrogenation enthalpy was reduced from 75.3 to 36.4 kJ/mol H_2 for MgH_2/Si system with 5% capacity [1]. In the mentioned cases, formation of more stable compound resulted in formation of a less stable or destabilized hydride upon hydrogenation according to the rule of

reversed stability [5]. However, despite achieving improved thermodynamics properties, the kinetics behavior of stabilized hydrides was still poor [1].

The model established by Griessen on relationship between the heat of formation of metal hydrides with the band structure energy difference has motivated research on changing the enthalpy by confining the equilibrium volume expansion upon hydrogenation [6]. In this case, Mg film constrained by layers of elements capable of forming stable alloy with Mg such as Ni and Pd show destabilization of hydride formation [7]. The destabilization is attributed to the elastic constraint or clamping effect exerted from formed alloy at the interface between Mg and the alloying element. Nonetheless, recent publication by Chung *et al.* attributed this destabilization to the chemical energy associated with Mg-Pd bonds in the layered film [8]. This is the same explanation described above for the chemical destabilization method in which formation of a more stable compound results in destabilization of its hydride. They argued that the strain energy effect resulted from constraining the volume expansion in the in-plane direction is insufficient to increase the plateau pressure substantially [8].

Aside from the chemical approach to destabilize the magnesium hydride, studies have been conducted to investigate the effect of early transition metals additives, which are immiscible with Mg, on the hydrogen sorption of its hydride [9, 10, 11, 12]. Experiments have shown considerable kinetics enhancements for $Mg_{(1-y)}-X_y$ ($X=Ti, V, Cr, Sc$) alloys, even though no significant thermodynamics alteration has been achieved [13]. The observed improvement in kinetics was correlated with the

formation of a fluorite-type hydride phase instead of the tetragonal rutile phase of MgH_2 for $y > 0.2$. For example, repeated (de)hydrogenation cycles have been reported for co-sputtered Mg-Ti thin films using electrochemical hydrogen sorption cycling method at room temperature [14]. Recent studies on $\text{MgH}_2/\text{TiH}_2$ system revealed the possibility of tuning thermodynamics properties of thin films in a multilayer structure [9, 15]. While there is an agreement with the fact that the degree of destabilization is strongly dependent on the magnesium thickness and Mg:Ti ratio, there are different explanations describing the mechanism of destabilization. Some groups attribute the destabilization to the strain induced by TiH_2 layer in the lattice of Mg and corresponding structural deformations [15, 16]. Others, on the other hand, correlate the observed destabilization to the contribution of interface energy to the total heat of hydride formation [9, 17]. Following is the model developed by Griessen [17] to explain the effect of interface energy. The energy associated with the formation of a new interface can contribute to the formation energy of the new phase. If we assume that the new phase is MgH_2 , the phase transformation is



The energy associated with the formation of this phase is the Gibbs free energy difference of the reaction:

$$\Delta_f G_{\text{MgH}_2}^0 = -RT \ln K = -RT \ln \left(\frac{P_{\text{bulk}}}{P^0} \right) \quad 3-2$$

Where K is the equilibrium constant, a function of P_{bulk} , the equilibrium hydrogen partial pressure of the hydride formation in bulk Mg. Considering that the system

consists of each Mg layer sandwiched between two layers of i (i =TiH₂), the change in the interfacial energy associated with the transformation of one Mg layer of area A to one MgH₂ layer of same area, can be written as:

$$\Delta_f G_{\text{nano}}^o = RT \ln \left(\frac{P_{\text{nano}}}{P^o} \right) = \Delta_f G_{\text{MgH}_2}^o + \sum A \gamma_{\text{MgH}_2|i} - \sum A \gamma_{\text{Mg}|i} \quad 3-3$$

Assuming that the interface energy is associated with certain crystallographic orientations of textured layers, in this case Mg(002)|TiH₂(111) for the dehydrogenated state and MgH₂(110)|TiH₂(111) for the hydrogenated state, we have

$$\ln \left(\frac{P_{\text{nano}}}{P_{\text{bulk}}} \right) = \frac{A \gamma_{\text{MgH}_2|i} - A \gamma_{\text{Mg}|i}}{RT} \quad 3-4$$

If the interface area between different layers is assumed to be constant and does not change upon hydrogenation which is the case for TiH₂, we have

$$\ln \left(\frac{P_{\text{nano}}}{P_{\text{bulk}}} \right) = \frac{A}{RT} \Delta \gamma \quad 3-5$$

The interface area per mole of thin film is proportional to the molar volume (V) of magnesium divided by its thickness d (V/d), and since each Mg layer is sandwiched between two layers, there are two interfaces contributing to the total energy of the system. Thus, A is equal to 2V/d.

$$\ln \left(\frac{P_d}{P_{\text{bulk}}} \right) = \frac{2V}{RTd} \Delta \gamma \quad 3-6$$

When the energy of the new interfaces is higher than that of original interfaces (Mg/TiH₂), $\Delta \gamma$ is positive and results in the destabilization of the hydride phase.

Using pressure-composition isotherms measurements of multilayers at different Mg thicknesses, one can measure the equilibrium pressure of the thin Mg layers (P_d), which is expected to be higher than that of bulk due to contributing effect of the interface. Therefore, considering equation 3-6 it is possible to calculate both $\Delta\gamma$ and P_{bulk} from a plot of $\ln(P_d)$ as a function of inverse thickness ($1/d$).

The effect of interface energy has been investigated in model thin films of Mg/TiH₂ deposited on a quartz substrate with very small mass loadings which could only be accurately measured using optical techniques [17]. In the present study, we synthesize sputtered multilayers with tens of layers which are peeled off the substrate and yield high mass loadings, good enough for accurate measurements using standard Sievert's apparatus. Our main goal is to investigate thermodynamics properties of Mg/AlTi multilayer system and compare the result to the baseline system (Mg/Ti multilayers). In fact, recent theoretical study predicts that incorporating Al or Si to Mg/Ti thin films can significantly improve their hydrogen storage properties [18]. Calculations show that the layered structure of Mg/TiSi or Mg/AlTi are more stable than co-sputtered ones (Mg/Ti-Al,Si alloys); thus, hydrides in the layered structure will be less stable than those in alloyed structures.

3.2 Experimental

Mg/AlTi and Mg/Ti multilayer thin films of total 0.5 μm thickness with various thicknesses of Mg and AlTi or Ti layers were prepared using Magnetron sputtering system (AJA International) on silicon wafers. AlTi layers were prepared through co-

sputtering of Al and Ti in 1:1 atomic ratio. All samples were coated with 7 nm Pd/AlTi bilayer to protect samples from oxidation and catalyze hydrogen dissociation and to prevent interdiffusion of Mg in Pd [19]. Deposition was performed under mean base pressure of 5×10^{-8} bar. For sputtering, argon gas of 99.999 % purity was used at pressure of 5 μ bar. Samples were removed from substrate by acetone dissolution of photoresist which has already been coated on the substrate.

Mg/AlTi and Mg/Ti samples were deposited at fixed 2 nm thickness of secondary layers (AlTi or Ti – unless mentioned otherwise) and various thicknesses of Mg layers. In addition, to further investigate the effect of size reduction and surface contribution in extreme cases, we prepared a different sample of Mg/AlTi with very low thicknesses of both AlTi and Mg layers as low as 0.5 nm. For simplicity we denote samples X/Y labels in which X is the thickness of magnesium and Y is the thickness of the secondary layers (AlTi or Ti) in nm.

A Sievert's apparatus (HyEnergy LLC. PCTPro 2000) was used to measure thermodynamics properties of the specimens. Test samples mass varied between 5 and 10 mg. A small 4 ml reservoir was used to set up the equilibrium pressure for both absorption and desorption processes. For samples with 2 nm secondary layers, thermodynamics measurements were run at 473 K, while for samples with thinner Mg layers, where the equilibrium pressure was higher than the pressure measurable accurately by low pressure transducer (around 5 atm), temperature was adjusted at a temperature between room temperature to 373 K.

To characterize the microstructure of as-prepared and hydrogen exposed samples, we used X-ray diffraction (XRD) and transmission electron microscopy (TEM). Focused ion beam (FIB) technique was used to prepare cross sectioned samples for TEM and a FIB-SEM (Zeiss NV vision 400 Focused Ion Beam equipped SEM) was used for preliminary characterization of multilayers and verify the soundness of the interfaces and thicknesses. The XRD system was a Bruker AXS diffractometer (Bruker Discover 8) operating with Cu-K α radiation. We performed TEM analysis using JEOL 2010 and JEOL 2200FS operating at 200 kV.

3.3 Results and discussion

X-ray diffraction patterns of the as deposited Mg/AlTi and Mg/Ti multilayers with different configurations can be seen in Figure 3-1a and 3-1b respectively. The textured structure of Mg is evident. It is already known that co-sputtered AlTi form a nanocrystalline/amorphous mixture with the main $\langle 111 \rangle$ peak at $2\theta=40^\circ$ [20]. While the initial dominant orientation seen in samples with Mg layers thinner than 2 nm is $\langle 0 1 1 \rangle$, it appears that $\langle 0 0 2 \rangle$ is the fastest growing orientation which is biased away from the initial orientation for thicker Mg layers (see ref. [21]). At Mg thickness of 2 nm, both orientations are observed. For 2/2 and 5/2 Mg/Ti multilayer configurations as can be seen in Figure 3-1b, X-ray diffraction patterns

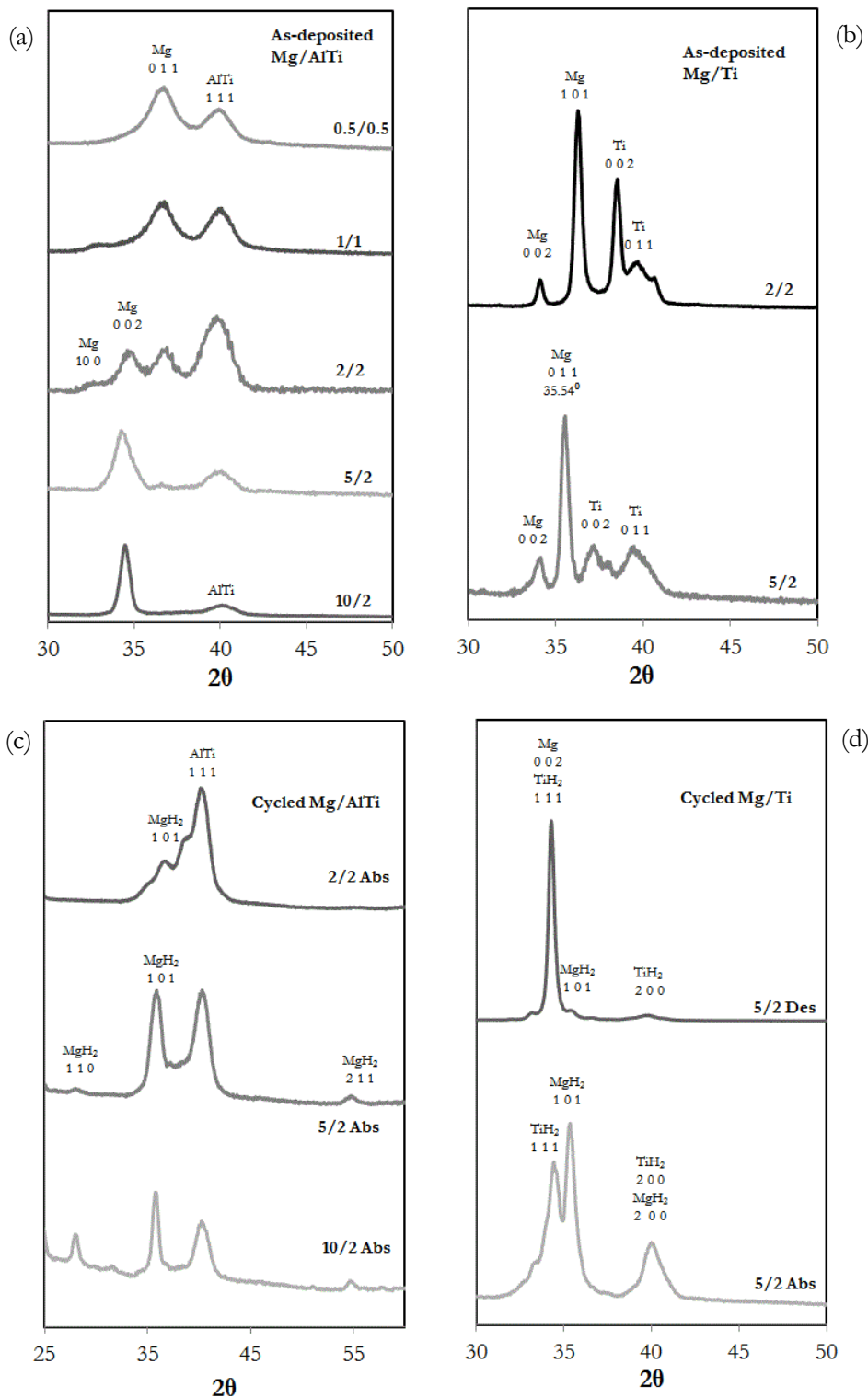


Figure 3-1 XRD patterns of as deposited Mg/AlTi samples of different configurations. At very thin thicknesses the preferred orientation for Mg changes from $\langle 0\ 2\ 2 \rangle$ to $\langle 0\ 1\ 1 \rangle$ (a) XRD patterns of as deposited 2/2 and 5/2 nm Mg/Ti samples (b) XRD patterns of Mg/AlTi samples after first absorption (c) and XRD patterns of 5/2 Mg/Ti after first absorption and first desorption (d).

indicate that $\langle 0\ 1\ 1 \rangle$ and $\langle 0\ 0\ 2 \rangle$ are the dominant growth direction for Mg and Ti layers, respectively.

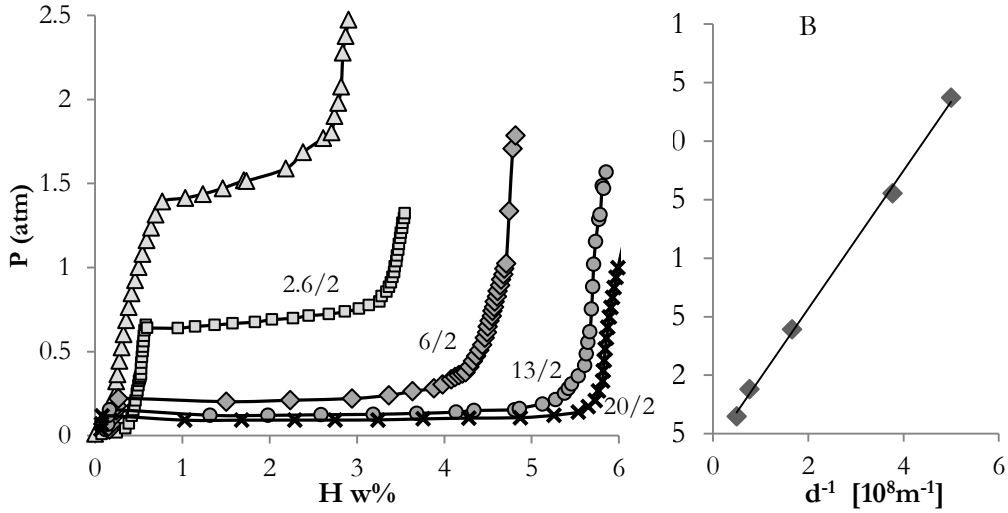


Figure 3-2 Absorption pressure – temperature isotherms of Mg-AlTi samples of three different Mg thicknesses (d) with constant AlTi thickness of 2 nm at 473 K (A) and the corresponding $\ln(P)$ as a function of $1/d$ (B).

Pressure–composition isotherms of Mg/AlTi multilayers at different thicknesses are shown in figure 3-2A. With decreasing the thickness of Mg, the equilibrium pressure becomes larger due to the increasing effect of interface energy, an effect which has been theoretically predicted in previous studies [18, 23]. The linear dependency of $\ln(P_d)$ versus inverse thickness ($1/d$) is depicted in Figure 3-2B. The fit gives values of 0.81 J/m^2 and 0.075 atm for $\Delta\gamma$ and P_{bulk} , respectively. The value for P_{bulk} is in agreement with the one obtained experimentally using enthalpy and entropy of bulk MgH_2 ($\Delta H = 74.06 \pm 0.42 \text{ kJ/mol H}_2$ and $\Delta S = 133.4 \pm 0.7 \text{ J/mol H}_2$) [22], which is 0.064 atm at 473 K.

The sloping plateau observed in the PCT of the multilayer with 2 nm Mg thickness is attributed to the fact that the Mg does not possess a single preferred orientation in

this sample; thus, there could be a range of interfacial energies contributing to the heat of formation that causes a short range sloping plateau. The calculated interface energies formations for $\text{Mg}|\text{TiH}_2$ and $\text{MgH}_2|\text{TiH}_2$ interfaces with different orientation relationships have been found to be the same in range [16]. This might explain why the sloping plateau is in a short pressure range as the difference in interface energies ($\Delta\gamma$) raised from distinct orientations of $\text{Mg}|\text{AlTi}$ and $\text{MgH}_2|\text{AlTi}$ is probably small.

It is worth mentioning that in our multilayer configurations, Mg layers can freely expand in the z direction and the effect of substrate is eliminated. In addition, all experiments were done at 473 K to enhance the kinetics and also minimize the hysteresis effect caused by plastic deformation; since according to Mooij et al, the hysteresis induces an increase in the plateau pressure in absorption and a decrease in equilibrium pressure in desorption which can be minimized at elevated temperatures [17]. Thus, we considered the absorption plateau pressures to calculate the interface energy.

Furthermore, we investigated the effect of decreasing the AlTi layer thickness, or in other words, increasing Mg:AlTi ratio, on the thermodynamics properties of Mg/AlTi films. It should be noted that any reduction in the AlTi layer thickness is accompanied with an increase in the hydrogen capacity which is favourable. Figure 3-3 depicts the PCT results for multilayers of 5 nm thick Mg and 8, 2 and 0.5 nm AlTi. All three samples have almost the same plateaus. The expected theoretical calculations imply that lower Mg:Ti ratio results in lower desorption energies, and

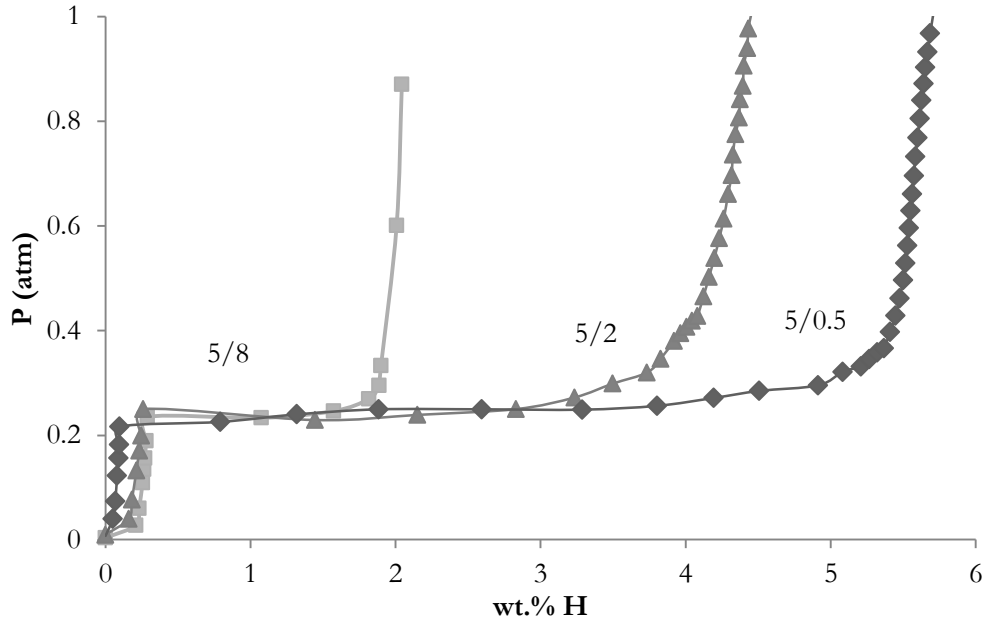


Figure 3-3 Absorption PCT of three multilayers with the Mg layers thickness constant at 5 nm and AlTi layers of 0.5, 2, and 8 nm measured at 473 K.

authors attribute this to the contributing effect of structural deformations rather than the positive interfacial energy effect [23]. Here, we could not find any significant change in PCT results of samples with different AlTi thicknesses, and hence the observed change in the equilibrium pressure could be merely caused by interfacial energy effect and it is thickness dependent.

To evaluate our thermodynamics results with those obtained from thin films on the substrate, we measured the thermodynamics properties of free standing Mg/Ti thin films as the baseline. Figure 3-4A depicts the PCT results for multilayer structure of 10, 5 and 2 nm Mg thick at fixed Ti thickness ($Ti = 2$ nm). Similar to Mg/AlTi, the higher plateau is achieved for lower Mg thickness. The more stability of Ti-H bonds dictates the presence of a lower plateau pressure for the hydride formation of titanium as can be seen in figure 3-4. This plateau can be clearly seen for three

samples with an expected more width for multilayers of low Mg thicknesses due to a higher Ti content. Upon hydrogenation, TiH_2 forms primarily in $\langle 111 \rangle$ direction (figure 1d) as reported elsewhere [9]. Thus, the interface affecting the thermodynamics property will be $\text{Mg}(101)|\text{TiH}_2(111)$. Figure 3-4B depicts the plot of $\ln(P_d)$ versus $1/d$ for Mg/Ti films giving the value of 0.44 J/m^2 for the interface energy difference which matches with the published result [17]. Thus, AlTi can contribute more energy to the heat of formation of hydride compared with Ti as predicted by theoretical calculations [18].

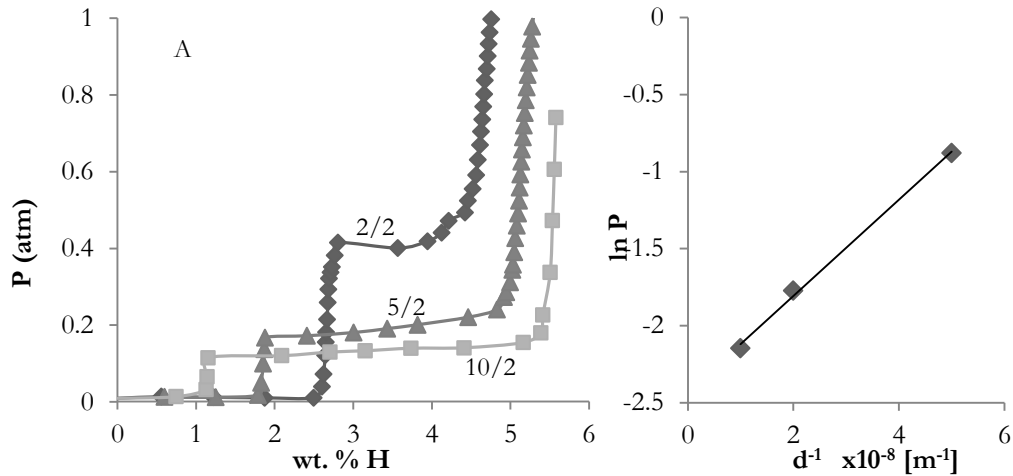


Figure 3-4 Absorption pressure – temperature isotherms of Mg-Ti samples of three different Mg thicknesses (d) with constant Ti thickness of 2 nm at 473 K (A) and the corresponding $\ln(p)$ as a function of $1/d$ (B).

The following absorption tests, we performed desorption PCT tests on the hydrided samples as can be seen in figure 3-5A. Neither Mg/Ti nor Mg/AlTi samples demonstrated a significant change in the thermodynamics of the desorption process. This could be attributed to the fact that Mg layers tend to disintegrate and detach from AlTi surface upon hydrogenation at high temperatures [24]. In such situation,

full contact between the AlTi and Mg is lost and Mg becomes pulverized. In fact, emergence of other diffraction peaks in the XRD pattern of Mg/AlTi and Mg/Ti samples in the absorbed state (Figure 3-1c and d) indicates that Mg(MgH₂) has lost the original textured/oriented structure with the AlTi layer. An SEM image (figure 3-5B) captured from a partially 2/2 Mg/AlTi multilayer reveals the disintegration of Mg at the interfaces in the top and bottom layers while the middle unabsorbed section remained intact.

In order to show the extreme amount of feasible destabilization, absorption PCT measurements were performed at room temperature (293 K) on a 0.5/0.5 Mg/AlTi

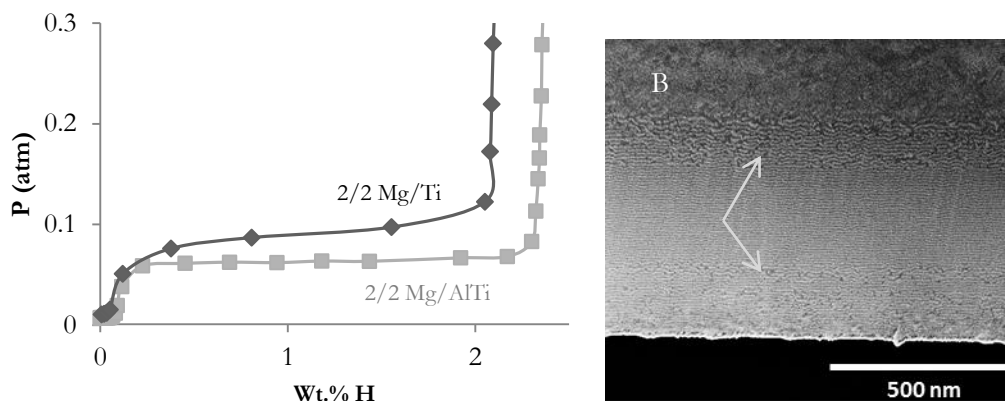


Figure 3-5 Desorption PCT of Mg/AlTi (2/2) and Mg/Ti (2/2) at 473 K (A). A SEM image of 2/2 Mg/AlTi after first absorption (B).

multilayer sample. The result is depicted in Figure 3-6A. The plateau pressure is around 0.05 atm corresponding to a formation enthalpy of 48 kJ/mol H₂. It was assumed that entropy of the reaction does not change. This enthalpy corresponds to a decomposition temperature of 75 °C at $P_{eq}=1$ bar. Note that the Mg/AlTi ratio for this sample is similar to 2/2 or 1/1 and the only difference is the configuration and periodicity of Mg/AlTi layers which in this sample is 1 nm. However, a significant

property change has been achieved by introducing more interfaces and their positive energy effect on the hydriding reaction. Interestingly for this sample, the kinetics is relatively fast. The absorption at room temperature occurs in less than 30 minutes and we were able to desorb the sample at 423 K in 25 minutes. The result of this experiment is shown in figure 3-6B and C. Similar low temperature sorption measurements have been investigated for co-sputtered thin films [25, 26]. Nonetheless, for multilayered structures, the reversibility of sorption processes and maintaining the achieved tuned properties should be investigated as their properties can be ruined at high temperatures due to the interface destruction.

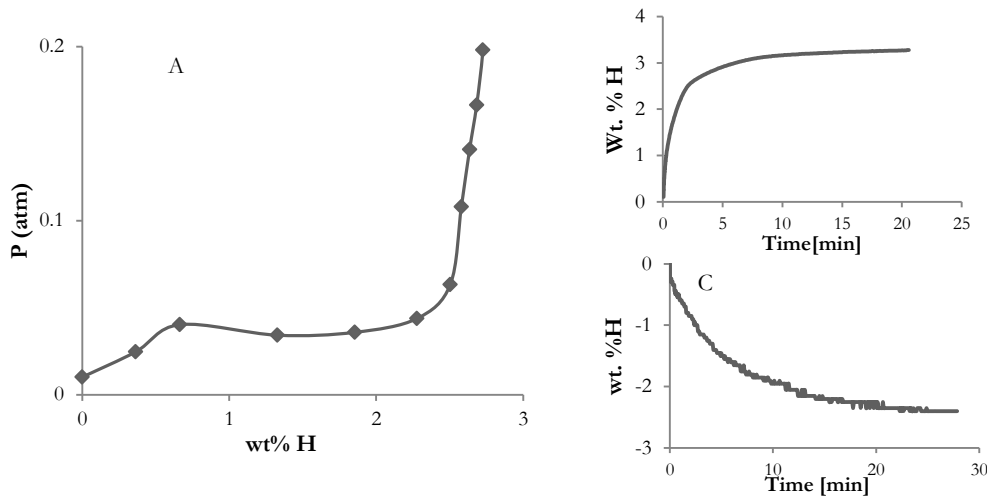


Figure 3-6 Absorption PCT of 0.5/0.5 Mg/AlTi measured at 293 K corresponding with enthalpy of 48 kJ/mole H₂ (A). Absorption (B) and desorption (C) curve at 293 K and 423 K respectively.

3.4 Summary

By making sputtered multilayers thin films where Mg layers are confined by secondary layers of AlTi (Ti), it was possible to scale up the destabilized structures where the interfacial energy between Mg and the secondary layer contributes to the

overall heat of hydride formation. The degree of destabilization is larger in the case of AlTi layers because of higher interface energy change during hydride nucleation on AlTi than on TiH₂. The amount of destabilization has a direct dependency on the thickness of Mg layer. The lower the thickness, the less the heat of hydride formation will be. Also, it was found that a change in the thickness of AlTi did not result in a significant change in the equilibrium pressure. Hence, by decreasing the thickness of AlTi layers, it is possible to maximize the capacity of material in a destabilized multilayer system.

3.5 References

- [1] J. J. Vajo, F. Mertens, C. C. Ahn, Bowman, and B. Fultz, "Altering Hydrogen Storage Properties by Hydride Destabilization through Alloy Formation: LiH and MgH₂ Destabilized with Si," *J. Phys. Chem. B*, vol. 108, no. 37, pp. 13977–13983, 2004.
- [2] X. Tan, M. Danaie, W. P. Kalisvaart, and D. Mitlin, "The influence of Cu substitution on the hydrogen sorption properties of magnesium rich Mg-Ni films," *International Journal of Hydrogen Energy*, vol. 36, no. 3, pp. 2154–2164, Feb. 2011.
- [3] S. Orimo and H. Fujii, "Materials science of Mg-Ni-based new hydrides," *Applied Physics A: Materials Science & Processing*, vol. 72, no. 2, pp. 167–186, 2001.
- [4] A. Zaluska, L. Zaluski, and J. O. Ström-Olsen, "Structure, catalysis and atomic reactions on the nano-scale: a systematic approach to metal hydrides for hydrogen storage," *Applied Physics A: Materials Science & Processing*, vol. 72, no. 2, pp. 157–165, 2001.
- [5] H. H. Van Mal, K. H. J. Buschow, and A. R. Miedema, "Hydrogen absorption in LaNi₅ and related compounds: Experimental observations and their

explanation,” *Journal of the Less Common Metals*, vol. 35, no. 1, pp. 65–76, Mar. 1974.

[6] R. Griessen and R. Feenstra, “Volume changes during hydrogen absorption in metals,” *Journal of Physics F: Metal Physics*, vol. 15, no. 4, pp. 1013–1019, Apr. 1985.

[7] A. Baldi, M. Gonzalez-Silveira, V. Palmisano, B. Dam, and R. Griessen, “Destabilization of the Mg-H System through Elastic Constraints,” *Phys. Rev. Lett.*, vol. 102, no. 22, p. 226102, Jun. 2009.

[8] C.-J. Chung, S.-C. Lee, J. R. Groves, E. N. Brower, R. Sinclair, and B. M. Clemens, “Interfacial Alloy Hydride Destabilization in Mg/Pd Thin Films,” *Phys. Rev. Lett.*, vol. 108, no. 10, p. 106102, Mar. 2012.

[9] A. Baldi, G. K. Pálsson, M. Gonzalez-Silveira, H. Schreuders, M. Slaman, J. H. Rector, G. Krishnan, B. J. Kooi, G. S. Walker, M. W. Fay, B. Hjörvarsson, R. J. Wijngaarden, B. Dam, and R. Griessen, “Mg/Ti multilayers: Structural and hydrogen absorption properties,” *Phys. Rev. B*, vol. 81, no. 22, p. 224203, Jun. 2010.

[10] G. Liang and R. Schulz, “Synthesis of Mg-Ti alloy by mechanical alloying,” *Journal of Materials Science*, vol. 38, no. 6, pp. 1179–1184, 2003.

[11] T. Takasaki, D. Kyoji, N. Kitamura, S. Tanase, and T. Sakai, “Reversible Hydrogen Storage Property and Structural Analysis for Face-Centered Cubic Hydride $Mg_{0.82}Zr_{0.18}H_2$ Prepared by Gigapascal Hydrogen Pressure Method,” *J. Phys. Chem. B*, vol. 111, no. 51, pp. 14102–14106, 2007.

[12] R. a. H. Niessen and P. H. L. Notten, “Electrochemical Hydrogen Storage Characteristics of Thin Film MgX ($X = Sc, Ti, V, Cr$) Compounds,” *Electrochem. Solid-State Lett.*, vol. 8, no. 10, pp. A534–A538, Oct. 2005.

[13] S. Er, D. Tiwari, G. A. de Wijs, and G. Brocks, “Tunable hydrogen storage in magnesium–transition metal compounds: First-principles calculations,” *Phys. Rev. B*, vol. 79, no. 2, p. 024105, Jan. 2009.

[14] P. Vermeulen, R. A. H. Niessen, and P. H. L. Notten, “Hydrogen storage in metastable $Mg_yTi_{(1-y)}$ thin films,” *Electrochemistry Communications*, vol. 8, no. 1, pp. 27–32, Jan. 2006.

[15] S. X. Tao, P. H. L. Notten, R. A. van Santen, and A. P. J. Jansen, “Fluorite transition metal hydride induced destabilization of the MgH_2 system in MgH_2/TMH_2

multilayers (TM=Sc, Ti, V, Cr, Y, Zr, Nb, La, Hf),” *Phys. Rev. B*, vol. 82, no. 12, p. 125448, 2010.

[16] S. Hao and D. S. Sholl, “Effect of TiH₂-Induced Strain on Thermodynamics of Hydrogen Release from MgH₂,” *J. Phys. Chem. C*, vol. 116, no. 2, pp. 2045–2050, 2011.

[17] L. P. A. Mooij, A. Baldi, C. Boelsma, K. Shen, M. Wagemaker, Y. Pivak, H. Schreuders, R. Griessen, and B. Dam, “Interface Energy Controlled Thermodynamics of Nanoscale Metal Hydrides,” *Advanced Energy Materials*, vol. 1, no. 5, pp. 754–758, 2011.

[18] S. Er, G. A. de Wijs, and G. Brocks, “Tuning the Hydrogen Storage in Magnesium Alloys,” *J. Phys. Chem. Lett.*, vol. 1, no. 13, pp. 1982–1986, 2010.

[19] X. Tan, C. T. Harrower, B. S. Amirkhiz, and D. Mitlin, “Nano-scale bi-layer Pd/Ta, Pd/Nb, Pd/Ti and Pd/Fe catalysts for hydrogen sorption in magnesium thin films,” *International Journal of Hydrogen Energy*, vol. 34, no. 18, pp. 7741–7748, Sep. 2009.

[20] M. Naka, T. Shibayanagi, M. Maeda, S. Zhao, and H. Mori, “Formation and physical properties of Al base alloys by sputtering,” *Vacuum*, vol. 59, no. 1, pp. 252–259, Oct. 2000.

[21] C. Ophus, E. J. Lubner, and D. Mitlin, “Analytic description of competitive grain growth,” *Physical review. E, Statistical, nonlinear, and soft matter physics*, vol. 81, no. 1.

[22] M. Paskevicius, D. A. Sheppard, and C. E. Buckley, “Thermodynamic Changes in Mechanochemically Synthesized Magnesium Hydride Nanoparticles,” *J. Am. Chem. Soc.*, vol. 132, no. 14, pp. 5077–5083, 2010.

[23] S.-X. Tao, P. H. L. Notten, R. A. van Santen, and A. P. J. Jansen, “Dehydrogenation properties of epitaxial (1 0 0) MgH₂/TiH₂ multilayers – A DFT study,” *Computational Materials Science*, vol. 50, no. 10, pp. 2960–2966, Aug. 2011.

[24] A. Baldi, V. Palmisano, M. Gonzalez-Silveira, Y. Pivak, M. Slaman, H. Schreuders, B. Dam, and R. Griessen, “Quasifree Mg–H thin films,” *Applied Physics Letters*, vol. 95, no. 7, pp. 071903–071903–3, Aug. 2009.

[25] B. Zahiri, M. Danaie, X. Tan, B. S. Amirkhiz, G. A. Botton, and D. Mitlin, “Stable Hydrogen Storage Cycling in Magnesium Hydride, in the Range of Room

Temperature to 300 °C, Achieved Using a New Bimetallic Cr-V Nanoscale Catalyst,”
J. Phys. Chem. C, vol. 116, no. 4, pp. 3188–3199, 2011.

[26] X. Tan, L. Wang, C. M. B. Holt, B. Zahiri, M. H. Eikerling, and D. Mitlin,
“Body centered cubic magnesium niobium hydride with facile room temperature
absorption and four weight percent reversible capacity,” Physical Chemistry
Chemical Physics, vol. 14, no. 31, p. 10904, 2012.

4 Conclusions

In this thesis, multilayers of Mg/AlTi thin films have been studied to investigate hydrogen storage properties. A significant enhancement in the kinetics and thermodynamics were achieved. There was an activation period before the thin films show a good kinetics behavior. This activation is relatively longer in comparison to the co-sputtered thin films. During activation, void formation and Mg pulverization were the main processes occurring simultaneously. This results in faster kinetics by exposing new Mg/AlTi surface to the hydrogen. Through appropriate construction of multilayers and thickness selection, we were able to achieve a material with 5.5 wt% H₂ capacity with long cycle life over 250 cycles. It was also found that addition of both Al and Ti to pure Mg layers has a significant effect on the stability of multilayered structure. TEM and EDX along with XRD results point out that Al and Ti segregated out during initial cycles and formed AlTi nanoparticles on surfaces or grain boundaries. We conclude that the AlTi addition to Mg and thickness reduction of Mg layers are the key factors in preventing structural deterioration.

It was also shown that decreasing the thickness of Mg layers to very few nanometers could potentially change the thermodynamics properties. By keeping the thickness of AlTi fixed at 2 nm and reducing the thickness of Mg layers, a less stable hydride was achieved. The destabilization is attributed to the effect of interface energy difference between Mg|AlTi and MgH₂|AlTi. Furthermore, the interface energy difference for Mg/AlTi system was found to be higher than that of Mg/Ti indicating that Al

addition to Mg/Ti system results in improved properties. Room temperature measurement for 0.5 nm thick Mg multilayer not only showed significant change in the thermodynamics properties, but also it demonstrated good kinetic behavior. The material absorbed in room temperature and could desorb at 423 K. However, further investigations are still required to achieve long cycle life stability.